

Journal Pre-proofs

Trinuclear *cis*-dioxidomolybdenum(VI) complexes of compartmental C_3 symmetric ligands: Synthesis, characterization, DFT study and catalytic application for hydropyridines (Hps) *via* the Hantzsch reaction

Mannar R. Maurya, Reshu Tomar, Puneet Gupta, Fernando Avecilla

PII: S0277-5387(20)30274-6
DOI: <https://doi.org/10.1016/j.poly.2020.114617>
Reference: POLY 114617

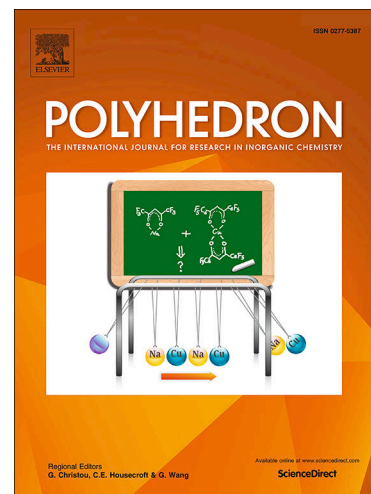
To appear in: *Polyhedron*

Received Date: 20 April 2020
Revised Date: 17 May 2020
Accepted Date: 19 May 2020

Please cite this article as: M.R. Maurya, R. Tomar, P. Gupta, F. Avecilla, Trinuclear *cis*-dioxidomolybdenum(VI) complexes of compartmental C_3 symmetric ligands: Synthesis, characterization, DFT study and catalytic application for hydropyridines (Hps) *via* the Hantzsch reaction, *Polyhedron* (2020), doi: <https://doi.org/10.1016/j.poly.2020.114617>

This is a PDF file of an article that has undergone enhancements after acceptance, such as the addition of a cover page and metadata, and formatting for readability, but it is not yet the definitive version of record. This version will undergo additional copyediting, typesetting and review before it is published in its final form, but we are providing this version to give early visibility of the article. Please note that, during the production process, errors may be discovered which could affect the content, and all legal disclaimers that apply to the journal pertain.

© 2020 Published by Elsevier Ltd.



Trinuclear *cis*-dioxidomolybdenum(VI) complexes of compartmental C_3 symmetric ligands: Synthesis, characterization, DFT study and catalytic application for hydroxyindoles (Hps) via the Hantzsch reaction

Mannar R. Maurya^{*,a}, Reshu Tomar^a, Puneet Gupta^a, Fernando Avecilla^b

^a *Department of Chemistry, Indian Institute of Technology Roorkee, Roorkee–247667, India. E-mail: m.maurya@cy.iitr.ac.in; Fax: +91 1332 273560; Tel: +91 1332 285327.*

^b *Grupo Xenomar, Centro de Investigaci3n Científicas Avanzadas (CICA), Departamento de Química, Facultade de Ciencias, Universidade da Coruña, Campus de A Coruña, 15071 A Coruña, Spain.*

Keywords:

Dioxidomolybdenum(VI) complexes
Structure elucidation
Homogeneous catalysis
Hantzsch reaction
DFT studies.

Highlights

1. Trinuclear dioxidomolybdenum(VI) complexes are reported.
2. The optimized structures deduced planar geometries of the complexes.
3. These complexes show excellent catalytic potential towards the one-pot three-components [ethyl acetoacetate, benzaldehyde (or its derivatives) and ammonium acetate] dynamic covalent assembly in the Hantzsch reaction.
4. With the elapse of time, the conversion of dihydroxyindole to the diethyl 2,6-dimethyl-4-phenylpyridine-3,5-dicarboxylate derivative occurs and completes in ca. 10 h with a distinct color change, showing the importance of the catalysts.

*Correspondence: Mannar R Maurya, E-mail: m.maurya@cy.iitr.ac.in; Fax: +91 1332 273560; Tel: +91 1332 285327

ABSTRACT

Trinuclear *cis*-dioxidomolybdenum(VI) complexes of the type $[\{\text{Mo}^{\text{VI}}\text{O}_2(\text{H}_2\text{O})\}_3\text{L}^{1-7}]$ (**1–7**) have been synthesized using tris(H_2ONO) donor ligands $[\text{H}_6\text{L}^{1-7}]$ (**I–VII**) assembled from benzene-1,3,5-tricarbohydrazide (bthz) and the corresponding salicylaldehyde (sal). All the ligands and the complexes were characterized by numerous techniques, such as FT-IR, UV-visible, NMR (^1H and ^{13}C) spectroscopy, electrochemical study, elemental analysis, thermogravimetric study and single crystal X-ray diffraction of the ligand **III** and complexes **1** and **5**. In the presence of H_2O_2 as an oxidant, these complexes show excellent catalytic potential towards the one-pot three-components [ethyl acetoacetate, benzaldehyde (or its derivatives) and ammonium acetate] dynamic covalent assembly in the Hantzsch reaction. Under solvent free conditions, as high as 98% conversion along with 100% selectivity towards diethyl 2,6-dimethyl-4-phenyl-1,4-dihydropyridine-3,5-dicarboxylate (1,4-DHP) has been achieved in 1 h. Although solvents do not improve the conversion, they do influence the selectivity of the products. With the elapse of time, the conversion of dihydropyridine to the diethyl 2,6-dimethyl-4-phenylpyridine-3,5-dicarboxylate derivative occurs and completes in ca. 10 h with a distinct color change, showing the importance of the catalysts. Efforts have been made to provide suitable reaction pathways for the catalytic reaction based on spectroscopic and density functional theory studies.

1. Introduction

High-valent dioxidomolybdenum(VI) complexes with a *cis*- $[\text{Mo}^{\text{VI}}\text{O}_2]$ core have had intense research focus in recent years due to their increased catalytic applications, e.g. oxygen atom transfer (OAT), olefin epoxidation, oxidation/ sulfoxidation, oxidative bromination [1] and some bio mimetic reactions [1b]. However, dinuclear and trinuclear dioxidomolybdenum(VI) complexes [2,3] with an open system, in which all metal centers are easily accessible to the substrate, may enhance their catalytic activity [3]. Such an idea inspired us to synthesize trinuclear dioxidomolybdenum(VI) complexes of tritopic phloroglucinol based ligands which have already been seen to show excellent catalytic activity in the oxidation of olefins [4].

Experimenting with the catalytic activity of such trinuclear molybdenum complexes for the aromatization of 1,4-dihydropyridine (1,4-DHP) via the one pot multicomponent Hantzsch reaction is an important task to take up as there are several new molecules having 1,4-DHP as

parent nuclei, which are clinically important drugs and used worldwide. Examples include Lercanidipine, Aranidipine, Cilnidipine, Efonidipine hydrochloride ethanol, Barnidipine hydrochloride, Lacidipine, Amlodipine besylate, Nisoldipine, Felodipine, Nimodipine etc. [5]. Apart from these, 1,4-DHPs are also used as a synthetic tool for selective $-C=C-$ reduction of α , β -unsaturated double bonds [6], endocyclic double bonds in coumarins [7], pyrazoles [8], $-C=N$ reduction in aldimines [9], quinolones [10], reductive cyclisation of allylic and benzylic bromides [11]. Further, the involvement of aromatized DHPs in the metabolic process during enzymatic oxidation also inspired researchers to synthesize their pyridine derivatives. Therefore, the synthesis of DHPs via the Hantzsch reaction and their aromatization have been carried out by numerous catalysts [12]. These catalysts require expensive reagents and challenging reaction conditions, but still end up with a low selectivity of the corresponding pyridine compound. In addition, the formation of the corresponding pyridine derivatives requires other oxidizing agents in the reaction, like $NaNO_2$ [13], metallic nitrates [14], CrO_2 [15], $Yb(OTf)_3$ [16], nitric acid [17], HZSM-5 zeolite [18], DDQ [19], bentonite clay [20], $KMnO_4$ [21], hyper valent iodine reagent [22], electrochemical oxidation [23], microwave [24] and simple air with a DMSO [25] supported catalyst with an ionic liquid layer (SCILL) [26] etc. Thus, researchers have moved towards metal complexes like Schiff based complexes of molybdenum [27,3e], vanadium [28] and manganese [29] and metal salts like $SbCl_5$ [30], $MoOCl_4$ [31], FeF_3 [32], $RuCl_3/O_2$ [33], $Co(OAc)_2/H_2O_2$ [34] etc. Due to the interest in synthesizing various DHPs and their corresponding pyridines, we have explored the catalytic activity of mononuclear and binuclear dioxidomolybdenum(VI) complexes towards the three component dynamic covalent assembly via the Hantzsch reaction [3e]. We have now successfully prepared a new series of trinuclear dioxidomolybdenum(VI) complexes with compartmental C_3 symmetric ligands based on benzene-1,3,5-tricarbohydrazide, (see Scheme 1). After complete characterization of these complexes, we have tested their catalytic activity for the aromatization of 1,4-dihydropyridine (1,4-DHP) via a one pot multicomponent Hantzsch reaction. We have optimized the reaction conditions to improve the catalytic activity of the synthesized complexes and to tune selectivity towards the pyridine derivative. We have also provided probable intermediates formed during the catalytic process using density functional theory computations.

<<Scheme 1>>

2. Experimental section

2.1. Materials, instrumentation and characterization procedures

All analytical reagent grade chemicals and solvents were obtained from standard sources and were used without further purification. The precursors benzene-1,3,5-tricarbohydrazide [35] and $[\text{Mo}^{\text{VI}}\text{O}_2(\text{acac})_2]$ [36] were prepared using standard reported procedures.

Elemental analyses (C, H and N) of the ligands and the complexes were performed with an Elementar model Vario-EL-III. IR Spectra were recorded in KBr discs on a Nicolet NEXUS Aligent 1100 FT-IR spectrometer. Electronic spectra of the ligands in DMSO and the complexes in MeOH were recorded using a Shimadzu 2450 UV-Vis spectrophotometer. ^1H and ^{13}C NMR spectra were obtained in DMSO- d_6 with a JEOL (400 MHz) spectrometer using the common parameter settings. Thermogravimetric analyses of the complexes were acquired using a TG Stanton Redcroft STA 780. The voltammograms of the ligands and the metal complexes were recorded in DMF between -1.8 and $+1.8$ V vs. SCE using 0.1 M TBAPF $_6$ as the supporting electrolyte with a 100 mV/s scan rate at room temperature. The catalytic reactions were monitored by a Shimadzu 2010 plus gas chromatograph fitted with a Rtx-1 capillary column ($30\text{ m} \times 0.25\text{ mm} \times 0.25\text{ }\mu\text{m}$) and an FID detector. The product formation was confirmed by a GC-MS model Perkin-Elmer, Clarus 500 by comparing the fragments of each product with the library available.

2.2. Preparations

2.2.1. Ligands H_6L^{1-7}

The ligands H_6L^{1-7} were prepared by similar methods. A representative method for **I** is presented here. A solution of salicylaldehyde (1.46 g, 12 mmol) in MeOH (30 mL) was added to a methanolic suspension of benzene-1,3,5-tricarbohydrazide (0.504 g, 2 mmol). The reaction mixture was refluxed on an oil bath. During this period, the benzene-1,3,5-tricarbohydrazide slowly dissolved and simultaneously a white solid precipitated. After 24 h of reflux, the reaction mixture was cooled at room temperature for an hour, the precipitated solid was filtered, washed with MeOH (2×5 mL) and dried in a desiccator over silica gel.

Data for H_6L^1 (**I**): Yield 0.954 g (85%). *Anal.* Calc. for $\text{C}_{30}\text{H}_{24}\text{N}_6\text{O}_6$ (564): C, 63.83; H, 4.29; N, 14.89. Found: C, 65.31; H, 4.82; N, 13.83%. IR data (cm^{-1}): 3440 (O-H), 3018 (N-H), 1659 (C=O), 1563 (C=N).

Data for H_6L^2 (**II**): Yield 0.920 g (51%). *Anal. Calc.* for $\text{C}_{54}\text{H}_{72}\text{N}_6\text{O}_6$ (901): C, 71.97; H, 8.05; N, 9.33. Found: C, 71.20; H, 8.23; N, 8.83%. IR data (cm^{-1}): 3270 (O–H), 2951 (N–H), 1660 (C=O), 1560 (C=N).

Data for H_6L^3 (**III**): Yield 0.980 g (75%). *Anal. Calc.* for $\text{C}_{33}\text{H}_{30}\text{N}_6\text{O}_9$ (654): C, 60.55; H, 4.62; N, 12.84. Found: C, 60.10; H, 4.41; N, 12.63%. IR data (cm^{-1}): 3436 (O–H), 3012 (N–H), 1642 (C=O), 1556 (C=N). Single crystals of **III** suitable for X-ray analysis were grown from DMF. The crystal of **III** is now formulated as $\text{H}_6\text{L}^3 \cdot 3\text{DMF}$ (**IIIa**).

Data for H_6L^4 (**IV**): Yield 1.00 g (82%). *Anal. Calc.* for $\text{C}_{30}\text{H}_{24}\text{N}_6\text{O}_9$ (612): C, 58.82; H, 3.95; N, 13.72. Found: C, 59.15; H, 4.20; N, 13.63%. IR data (cm^{-1}): 3438 (O–H), 2980 (N–H), 1678 (C=O), 1552 (C=N).

Data for H_6L^5 (**V**): Yield 0.846 g (63%). *Anal. Calc.* for $\text{C}_{30}\text{H}_{21}\text{Cl}_3\text{N}_6\text{O}_6$ (667): C, 53.95; H, 3.17; N, 12.58. Found: C, 53.60; H, 3.32; N, 12.63%. IR data (cm^{-1}): 3422 (O–H), 3010 (N–H), 1661 (C=O), 1560 (C=N).

Data for H_6L^6 (**VI**): Yield 0.918 g (76%). *Anal. Calc.* for $\text{C}_{33}\text{H}_{30}\text{N}_6\text{O}_6$ (606): C, 65.34; H, 4.98; N, 13.85. Found: C, 65.10; H, 4.60; N, 13.48%. IR data (cm^{-1}): 3434 (O–H), 2989 (N–H), 1671 (C=O), 1567 (C=N).

Data for H_6L^7 (**VII**): Yield 0.992 g (64%). *Anal. Calc.* for $\text{C}_{42}\text{H}_{51}\text{N}_9\text{O}_6$ (777): C, 64.85; H, 6.61; N, 16.20. Found: C, 64.45; H, 6.33; N, 16.61%. IR data (cm^{-1}): 3442 (O–H), 3015 (N–H), 1653 (C=O), 1558 (C=N).

2.2.2. $[\{\text{Mo}^{\text{VI}}\text{O}_2(\text{MeOH})\}_3\text{L}^1]$ (**I**)

To a suspension of **I** (0.564 g, 1 mmol) in MeOH (20 mL) was added a filtered solution of $[\text{Mo}^{\text{VI}}\text{O}_2(\text{acac})_2]$ (1.14 g, 3.5 mmol) in dry/absolute MeOH (20 mL) with stirring, whereupon the ligand dissolved within a few minutes. The orange solution was refluxed on a water bath for 6 h. The yellow solid that separated after cooling the reaction mixture to room temperature for 1 h was collected by filtration, washed with cold MeOH followed by petroleum ether and dried in a desiccator over silica gel. Yield 0.920 g (89%). *Anal. Calc.* for $\text{C}_{33}\text{H}_{30}\text{Mo}_3\text{N}_6\text{O}_{15}$ (1038.51): C, 38.17; H, 2.91; N, 8.09. Found: C, 38.12; H, 2.94; N, 8.07%. IR data (cm^{-1}): 3450 (O–H), 1550 (C=N), 1248 (C–O), 923 (O=Mo=O)_{asym}, 901 (O=Mo=O)_{sym}. Single crystals of **1** suitable for X-ray analysis were grown from DMSO. The crystal of complex **1** is now formulated as $[\{\text{MoO}_2(\text{DMSO})\}_3\text{L}^1]$ (**1a**).

2.2.3. $[\{Mo^{VI}O_2(MeOH)\}_3L^2]$ (**2**)

Complex **2** was prepared from **II** (0.901 g, 1 mmol) in MeOH (20 mL) and a filtered solution of $[Mo^{VI}O_2(acac)_2]$ (1.14 g, 3.5 mmol) in dry/absolute MeOH (20 mL) following the procedure outlined for **1**. Yield 1.010 g (74%). *Anal.* Calc. for $C_{57}H_{78}Mo_3N_6O_{15}$ (1375.15): C, 49.79; H, 5.72; N, 6.11. Found: C, 49.72; H, 5.70; N, 6.13%. IR data (cm^{-1}): 3430 (O–H), 1508 (C=N), 1256 (C–O), 921 (O=Mo=O)_{asym}, 905 (O=Mo=O)_{sym}.

2.2.4. $[\{Mo^{VI}O_2(MeOH)\}_3L^3]$ (**3**)

This complex was prepared similarly as reported for **1** from $[Mo^{VI}O_2(acac)_2]$ (1.14 g, 3.5 mmol) and **III** (0.654 g, 1 mmol) in dry/absolute MeOH. Yield 0.820 g (73%). *Anal.* Calc. for $C_{36}H_{36}Mo_3N_6O_{18}$ (1128.58): C, 38.31; H, 3.22; N, 7.45. Found: C, 38.32; H, 3.24; N, 7.42%. IR data (cm^{-1}): 3450 (O–H), 1540 (C=N), 1262 (C–O), 932 (O=Mo=O)_{asym}, 904 (O=Mo=O)_{sym}.

2.2.5. $[\{Mo^{VI}O_2(MeOH)\}_3L^4]$ (**4**)

Complex **4** was prepared in dry/absolute MeOH using $[Mo^{VI}O_2(acac)_2]$ (1.14 g, 3.5 mmol) and **IV** (0.612 g, 1 mmol) adopting the method reported for **1**. Yield 0.934 g (86%). *Anal.* Calc. for $C_{33}H_{30}Mo_3N_6O_{18}$ (1086.50): C, 36.48; H, 2.78; N, 7.74. Found: C, 36.42; H, 2.74; N 7.75%. IR data (cm^{-1}): 3470 (O–H), 1541 (C=N), 1264 (C–O), 933 (O=Mo=O)_{asym}, 909 (O=Mo=O)_{sym}.

2.2.6. $[\{Mo^{VI}O_2(MeOH)\}_3L^5]$ (**5**)

Complex **5** was prepared in dry/absolute MeOH using $[Mo^{VI}O_2(acac)_2]$ (1.14 g, 3.5 mmol) and **V** (0.667 g, 1 mmol) adopting the method reported for **1**. Yield 0.900 g (79%). *Anal.* Calc. for $C_{33}H_{27}Mo_3Cl_3N_6O_{15}$ (1141.83): C, 34.71; H, 2.38; N, 7.36. Found: C, 34.72; H, 2.33; N, 7.32%. IR data (cm^{-1}): 3445 (O–H), 1542 (C=N), 1254 (C–O), 940 (O=Mo=O)_{asym}, 910 (O=Mo=O)_{sym}. Single crystals of **5** suitable for X-ray analysis were grown from DMSO-DMF (1:9). The crystal of complex **5** is now formulated as $[\{MoO_2(0.5H_2O \cdot 0.5MeOH)\}\{MoO_2(DMF)\}\{MoO_2(DMSO)\}L^2] \cdot DMF \cdot 0.5DMSO$ (**5a**).

2.2.7. $[{\text{Mo}}^{\text{VI}}\text{O}_2(\text{MeOH})_3\text{L}^6]$ (**6**)

Complex **6** was prepared in dry/absolute MeOH using $[\text{Mo}^{\text{VI}}\text{O}_2(\text{acac})_2]$ (1.14 g, 3.5 mmol) and **VI** (0.606 g, 1 mmol) adopting the method reported for **1**. Yield 0.860 g (80%). *Anal.* Calc. for $\text{C}_{36}\text{H}_{36}\text{Mo}_3\text{N}_6\text{O}_{15}$ (1080.59): C, 40.01; H, 3.36; N 7.78. Found: C, 40.02; H, 3.33; N, 7.72%. IR data (cm^{-1}): 3448 (O–H), 1547 (C=N), 1265 (C–O), 943 (O=Mo=O)_{asym}, 912 (O=Mo=O)_{sym}.

2.2.8. $[{\text{Mo}}^{\text{VI}}\text{O}_2(\text{MeOH})_3\text{L}^7]$ (**7**)

Complex **7** was prepared in dry/absolute MeOH using $[\text{Mo}^{\text{VI}}\text{O}_2(\text{acac})_2]$ (1.14 g, 3.5 mmol) and **VII** (0.777 g, 1 mmol) following the method reported for **1**. Yield 0.860 g (69%). *Anal.* Calc. for $\text{C}_{45}\text{H}_{57}\text{Mo}_3\text{N}_9\text{O}_{15}$ (1251.87): C, 43.17; H, 4.59; N, 10.07. Found: C, 43.12; H, 4.53; N, 10.02%. IR data (cm^{-1}): 3451 (O–H), 1538 (C=N), 1257 (C–O), 934 (O=Mo=O)_{asym}, 908 (O=Mo=O)_{sym}.

2.3. X-ray crystal structure determination

Three-dimensional X-ray data were collected on a Bruker Kappa Apex CCD diffractometer at low temperature for compounds **III**, **1** and **5** by the ϕ - ω scan method. Reflections were measured from a hemisphere of data collected from frames, each of them covering 0.3° in ω . A total of 82697 for **III**, 41831 for **1** and 89803 for **5** measured reflections were corrected for Lorentz and polarization effects and for absorption by multi-scan methods based on symmetry-equivalent and repeated reflections. Of the total, 6848 for **III**, 3373 for **1** and 6809 for **5** independent reflections exceeded the significance level ($|F|/\sigma|F|$) > 4.0. After data collection, in each case a multi-scan absorption correction (SADABS) [37] was applied, and the structures were solved by direct methods and refined by full matrix least-squares on F^2 data using the SHELX suite of programs [38]. Hydrogen atoms were included in calculated positions and refined in the riding mode in **1** and **5**. In **5**, some hydrogen atoms of solvent molecules were not located due to disorder. In **III**, hydrogen atoms were located in the difference Fourier map and left to refine freely, except for C(1D), O(2), C(2D), C(4D), C(5D), C(6D), C(7D), O(8), C(8D), C(15), C(24) and C(33), which were included in calculated positions and refined in the riding mode. Refinements were done with allowance for thermal anisotropy of all non-hydrogen atoms, except for O(3DB), due to the disorder of this DMF molecule.

The DMSO molecule coordinated to the Mo atom in **1** presents an important disorder. This disorder has been refined and two atomic sites have been observed and refined with anisotropic

atomic displacement parameters for the methyl and sulfur atoms of DMSO. More specifically this disorder was refined using 49 restraints (SADI, SIMU and DELU restraints were used). The site occupancy factor was 0.62165 for S(1A)-C(1MA)-C(2MA). In **5**, a water or methanol molecule occupies a coordination position and the disorder was refined. The site occupancy factor was 0.72545 for O(1WA). A final difference Fourier map of **III** showed no residual density outside 0.834 and -0.267 e Å⁻³.

For **1**, a final difference Fourier map showed an important residual density, 4.248 and -1.013 e Å⁻³, next to the DMSO molecule coordinated to the Mo atom, due to the slip plane that contains a symmetrical spatial group, such as R $\bar{3}$, and the impossibility of locating a third disorder position for the S(1), C(1M) and C(2M) atoms of DMSO. For **5**, the final difference Fourier map showed high values due to the disorder of the solvent molecules, which could be refined: 1.706 and -1.229 e Å⁻³. Weighting schemes $w = 1/[\sigma^2(F_o^2) + (0.096600 P)^2 + 0.103000 P]$ for **III**, $1/[\sigma^2(F_o^2) + (0.106900 P)^2 + 160.176315 P]$ for **1** and $1/[\sigma^2(F_o^2) + (0.177300 P)^2 + 0.000000 P]$ for **5**, where $P = (|F_o|^2 + 2|F_c|^2)/3$, were used in the latter stages of refinement. Further details of the crystal structure determinations are given in Table 1.

<<Table 1>>

2.4. Computational details

All calculations were performed using the ORCA quantum chemical program package [39]. Geometries were optimized with the hybrid-GGA (generalized gradient approximation) density functional B3LYP [40] in conjunction with def2-TZVP(-f) basis sets [41], without f polarization functions. To accelerate the overall calculations, the RIJCOSX [42] (resolution-of-the-identity for Coulomb (RIJ) with a chain of sphere (COS) algorithm for the Hartree-Fock (HF) exchange (X) part) approximation was applied for the expensive integral calculations. Non-covalent interactions were accounted for by using atom-pairwise dispersion corrections with Becke-Johnson (D3BJ) damping [43]. Subsequent numerical frequency calculations were undertaken for the optimized geometries to confirm that they correspond to stationary points featuring no imaginary frequencies. The zero-point vibrational energies, thermal corrections and entropy terms were obtained from the frequency calculations.

2.5. Catalytic activity study: One-pot three-component dynamic covalent assembly via the Hantzsch reaction

All the catalytic reactions were carried out following a general procedure. In a typical reaction, benzaldehyde (0.53 g, 0.0050 mol), ethyl acetoacetate (1.1 g, 0.010 mol) and ammonium acetate (0.38 g, 0.0050 mol) were mixed together in a 50 mL round-bottom two necked glass reaction flask assembled with a water cooled reflux condenser. The appropriate catalyst (0.0010 g) and aqueous 30% H₂O₂ (0.005, 0.010 or 0.015 mol) under solvent free conditions were added and the reaction mixture was stirred at a fixed temperature using an oil bath. The progress of the reaction was examined by taking out small aliquots of the reaction mixture, extracting with n-hexane and injecting into the GC column. The identities of the products were confirmed by GC-MS, HRMS and ¹H NMR spectroscopy.

3. Results and discussions

Reaction of benzene-1,3,5-tricarbohydrazide [36] with different derivatives of salicylaldehyde in a 1:3 molar ratio in a MeOH suspension resulted in the formation of the analytically pure ligands **I–VII** in good yields (Scheme 1). A suspension of these ligands in MeOH react with [Mo^{VI}O₂(acac)₂] [37] in a 1:3 molar ratio under reflux conditions to give the corresponding trinuclear dioxidomolybdenum(VI) complexes [{Mo^{VI}O₂(MeOH)₃L¹}] (**1**), [{Mo^{VI}O₂(MeOH)₃L²}] (**2**), [{Mo^{VI}O₂(MeOH)₃L³}] (**3**), [{Mo^{VI}O₂(MeOH)₃L⁴}] (**4**), [{Mo^{VI}O₂(MeOH)₃L⁵}] (**5**), [{Mo^{VI}O₂(MeOH)₃L⁶}] (**6**) and [{Mo^{VI}O₂(MeOH)₃L⁷}] (**7**) of high C₃-symmetry. Scheme 2 presents the proposed structure of the complexes, which are based on various evidences whose descriptions are presented below.

<<Scheme 2>>

3.1. Description of the molecular structures of the compounds

ORTEP diagrams for the compounds **IIIa**, **1a** and **5a** (**IIIa**, **1a** and **5a** are the crystallised forms of **III**, **1** and **5**, respectively) are shown in Figs. 1, 2 and 3, respectively. Details of the crystal structure determinations are given in the supporting information. Selected bond distances and angles of these structures are given in Table 2.

Compound **IIIa** crystallizes with three DMF molecules. In the crystal packing (see Fig. S1) the principal interactions between the molecules are hydrogen bonds (see Table 3) and C-O $\cdots\pi$ interactions. The distance between the O(5H) atom and the next phenyl ring of another molecule, $d_{\text{O(5H)-c5}}$ [c5, C(18I)-C(19I)-C(20I)-C(21I)-C(22I)-C(23I)], is 3.500(3) Å and the distance between the O(4H) atom and the centroid situated in the middle of hydrazone group, [c6, N(3H)-N(4H)], is 3.402 Å. Each arm of the ligand is essentially planar [mean deviation from planarity of the atoms C(7), C(8), C(9), C(10), C(11), C(12), C(13), C(14), N(1), N(2), O(1) and O(2), plane 1, 0.0242(25) Å; C(16), C(17), C(18), C(19), C(20), C(21), C(22), C(23), N(3), N(4), O(4) and O(5), plane 2, 0.0513(22) Å; C(25), C(26), C(27), C(28), C(29), C(30), C(31), C(32), N(3), N(4), O(7) and O(8), plane 3, 0.1407(21) Å], but the three arms are not coplanar. The dihedral angles between the arms are, 13.54(9)° between planes 1 and 2, 16.98(7)° between planes 2 and 3, and 3.45(8)° between planes 3 and 1.

<<Figure 1>>

The molecular structures of compounds **1a** and **5a** present trinuclear complexes which are best described as having a six-coordinated distorted octahedral geometry around each Mo center. These structures present a high C_3 -symmetry, with a phenyl group in the center and three arms where the Mo atoms appear coordinated. Each Mo atom is coordinated by two oxide atoms of the dioxido cis-[Mo^{VI}O₂] moiety [Mo(1)-O(1), 1.710(4) Å and Mo(1)-O(2), 1.694(5) Å in **1a** and Mo(1)-O(1), 1.697(7) Å and Mo(1)-O(2), 1.686(7) Å in **5a**], like in other similar compounds. All the Mo=O bonds are similar to each other in regard to their bond lengths and have the characteristic oxido-type O atoms. The equatorial planes are occupied by one nitrogen atom and three oxygen atoms, one of which is a Mo=O bond [Mo-O(1)]. The other three atoms belong to the ligand around each Mo center. The last axial position is occupied by one oxygen atom of a DMSO molecule in **1a** and of H₂O or MeOH, DMF and DMSO in **5a**. Again, each arm of the ligand is essentially planar [mean deviation from planarity of the atoms C(3), C(4), C(5), C(6), C(7), C(8), C(9), C(10), N(1), N(2), O(3) and O(4), 0.0428(50) Å in **1a** and C(7), C(8), C(9), C(10), C(11), C(12), C(13), C(14), N(1), N(2), O(3) and O(4), 0.0655(75) Å, C(15), C(16), C(17), C(18), C(19), C(20), C(21), C(22), N(3), N(4), O(7) and O(8), 0.0344(6) Å and C(23), C(24), C(25), C(26), C(27), C(28), C(29), C(30), N(5), N(6), O(11) and O(12), 0.0839 Å in **5a**], but the three arms are not coplanar. The dihedral angles between the planes defined for the arms were measured and identical angles

of $26.9(3)^\circ$ were found due to the high symmetry. These positions of the arms and the coordination of the DMSO molecule, which is situated in the holes between the complexes, limit the interaction between them in the crystal packing in **1a** (see Fig. S2). In **5a**, two of the arms [C(15)-C(22), N(3), N(4), O(7), O(8) and C(23)-C(30), N(5), N(6), O(11), O(12)] are approximately co-planar with a dihedral angle of $2.67(5)^\circ$ between them, and the third arm [C(7)-C(14), N(1), N(2), O(3), O(4)] makes angles of $11.73(4)$ and $14.3(6)^\circ$ with the first two arms, respectively. Additionally, arms in adjacent molecules show π - π stacking interactions between them (see Fig. S3).

<<Figures 2 and 3>> <<Tables 2 and 3>>

3.2. Thermal study

In general, the thermal analyses of the complexes show their stability up to 100°C and then their mass reduces exothermically between 100 and 167°C , which is equivalent to three coordinated MeOH molecules, indicating their coordination to the molybdenum atoms. Upon a further increase in temperature, the anhydrous complexes decompose exothermically in two to three overlapping steps and form MoO_3 at ca. 530°C . Fig. 4 provides the TGA profiles of complexes **2** and **4** with the mass lost at the two major stages.

<<Figure 4>>

3.3. FT-IR spectroscopic studies

In order to confirm the coordinating functionalities, the IR spectra of the free ligands were compared with the corresponding metal complexes and the results are listed in Table S1. The IR spectra of the ligands register two broad bands at 3018 - 3167 and 1617 - 1648 cm^{-1} due to $\nu(\text{NH})$ and $\nu(\text{C}=\text{O})$ (of the hydrazide moiety) stretches, respectively. The absence of these bands and the appearance of a new band at ca. 1250 cm^{-1} in the metal complexes are in line with the enolization of the ketonic groups of the hydrazide moieties followed by coordination of the enolate oxygen atoms. The coordination of phenolic oxygen atom cannot be revealed unequivocally due to the presence of a methanol molecule [$\nu(\text{O}-\text{H})$ at 3424 - 3450 cm^{-1}] associated with the complexes. However, the coordination of the phenolic oxygen atom after deprotonation has been confirmed in **1a** and **5a** by the single crystal X-ray study (vide supra). All these complexes exhibit two prominent IR bands at 921 - 943 and 901 - 912 cm^{-1} , which are assigned to $\nu_{\text{asym}}(\text{O}=\text{Mo}=\text{O})$ and $\nu_{\text{sym}}(\text{O}=\text{Mo}=\text{O})$ modes, respectively due to the *cis*-[MoO_2] structure [44]. Further, only two sharp

peaks in all the complexes for these modes suggest that the Mo centers in the tris[*cis*-MoO₂]-complexes are arranged in a symmetrical fashion.

3.4. UV/Vis spectroscopic studies

The electronic absorption spectra of the ligands and their tris[*cis*-MoO₂]-complexes were recorded in DMSO due to their poor solubility in other solvents. Their absorption maxima and extinction coefficients are listed in Table S2. All the ligands exhibit three bands at 290-299, 302-309 and 330-346 nm (Fig. S4). First two bands seem to be split bands of a $\pi \rightarrow \pi^*$ transition as they have almost the same extinction coefficient, while last band is assignable to a $n \rightarrow \pi^*$ transition. In most cases, the $n \rightarrow \pi^*$ transition shifts to a lower wavenumber upon coordination of the ligands to the metal ion due to a structural rearrangement within the ligand, while the other two bands collapse and appear as a single band at a lower wavelength. In addition, a new band is generated at 420–488 nm in all the complexes due to charge transfer of electrons from the filled p-orbitals of the ligand to the vacant d-orbitals of the metal ion (L \rightarrow M) in the proper orientation.

3.5. ¹H and ¹³C NMR spectroscopic studies

The coordination behavior of the ligands towards the molybdenum ion was ascertained by comparing their ¹H NMR spectra with those of the corresponding complexes. The ¹H NMR spectral data of the ligands and the complexes, acquired in DMSO-d₆, are collected in Table 4 along with the J values for the aromatic protons and representative spectra (e.g. of ligand **I** and complex **1**) of the series are reproduced in Fig. S5. A sharp signal at δ 12.22-12.92 ppm in the ligands' spectra is indicative of their existence in the ketonic form. The absence of this signal in the spectra of all the complexes is in accordance with the enolization of the ketonic group of the ligands followed by coordination of the enolate O atoms to the Mo atoms. Similarly, the absence of a phenolic proton in the complexes, that appears at δ 11.16-12.61 ppm in the ligands, suggests the coordination of all three phenolate oxygen atoms to the Mo atoms. The protons of the azomethine group and benzene ring of the hydrazide moiety resonate at ca. δ 8.73 ppm in the ligands, but in the complexes, the azomethine protons' signals shift considerably downfield while the signals for the aromatic protons remain almost unchanged. The downfield shift of the azomethine proton signifies the coordination of azomethine nitrogen atom. Other aromatic protons of the ligands and the complexes appear within the expected regions, with only slight variations.

Thus, the binding behavior of each unit of ligands is ONO dibasic tridentate in all the metal complexes.

<<Table 4>>

The coordination behavior of the ligands towards the tris[*cis*-MoO₂] complexes was further confirmed by comparing the ¹³C NMR data of all the ligands with their complexes. The ¹³C NMR spectra of the representative ligand **I** and complex **1** are given in Fig. S6 and the complete data are collected in Table S3. The coordination of the O, N and O atoms of each pocket of the ligands to the metal ion has direct influence on the carbon atoms present in the vicinity of these coordination functionalities due to adjustment of the electronic environment. Thus significant coordination-induced ¹³C NMR chemical shifts [$\Delta\delta = \delta(\text{complex}) - \delta(\text{ligand})$] for the carbon atoms associated with the phenolic oxygen atoms (C6/C6'/C6'') ($\Delta\delta = 2.3 - 7.67$ ppm), the azomethine nitrogen atoms (C4/C4'/C4'') ($\Delta\delta = 2.93 - 8.59$ ppm) and enolic oxygen atoms (C3/C3'/C3'') ($\Delta\delta = 2 - 12.71$ ppm) have been observed (Table 3) due to coordination of these atoms. Other carbon atoms, i.e. C9/C9'/C9'', C7/C7'/C7'', C10/C10'/C10'', C8/C8'/C8'', C2/C2'/C2'', C1/C1'/C1'', C5/C5'/C5'' are also affected, but only slightly, due to electronic rearrangements. In complexes **2**, **3**, **6** and **7**, a new signal also appears at δ 47.87, 20.43, 20.50 and 56.32 ppm due to the presence of CH₂-CH₃, CH₃ and OMe groups, respectively.

3.6. Electrochemical properties

The cyclic voltammetry (CV) and differential pulse voltammetry (DPV) of ligands **I-VII** and complexes **1-7** were studied in DMF solution to explore their redox behavior in the solution state (Table 5). Representative cyclic voltammograms and differential pulse voltammograms of **I** and **1** are presented in Fig. 5. The CV trace of complex **1** displays two cathodic peaks at -1.02 and -0.732 V due to the Mo(VI) → Mo(V) reduction and the redox behavior of the ligand, respectively. The nature of the later peak was confirmed by analyzing the CV of ligand **I** recorded in the same range, which displays an oxidative peak at 0.613 V and a reductive peak at -0.715 V. The first cathodic peak is well within the range reported for dioxidomolybdenum(VI) complexes of dibasic tetradentate salen type ligands, but it is a little lower than the range observed for trinuclear dioxidomolybdenum(VI) complexes of tritopic 2,4,6-triacetylphloroglucinol based ligands [45]. The reductive peaks of the complex are irreversible in nature in polar aprotic solvents, corresponding to the Mo(VI)/Mo(V) reduction [46]. The oxidative peak due to metal-centered

oxidation of the molybdenum complex is not observed during the anodic scan, probably due to the fast decomposition of the reduced species [45, 47].

In order to support the above data, the DPV was also recorded immediately after the CV trace at the same scan rate. It was witnessed that the reduction peaks at -1.13 and -0.715 V and oxidation peak at 0.613 V of the ligand **I** in the CV do not match exactly with the corresponding peaks at -0.878 and 0.486 V in the DPV. Similarly, peaks at -1.02 , and -0.732 V in the CV and at -0.892 , -0.112 and 0.599 V in the DPV of complex **1** do not match. This information confirms that both the systems (i.e. the ligand as well as the complex) are irreversible in nature in DMF solution. The peaks are unsymmetrical in both cases, which again concludes the irreversible nature of the system. The CV and DPV of all other complexes display comparable patterns (Figs. S7-S12). A metal centered oxidation peak is not observed either in the CV traces or in the DPV traces.

<<Table 5>> <<Figure 5>>

3.7. Catalytic activity study – the Hantzsch reaction

An efficient one pot Hantzsch reaction of three components involving ethyl acetoacetate, benzaldehyde (or its derivatives) and ammonium acetate has been explored using complexes **1-7** as catalysts under solvent free conditions in the presence of a green oxidant, i.e. 30% H_2O_2 . Literature, in general, reports the formation of as many as four products (Scheme 3) [48], however, the mononuclear $[\text{Mo}^{\text{VI}}\text{O}_2]^{2+}/[\text{Mo}^{\text{VI}}\text{O}(\text{O}_2)]^{2+}$ and $[\text{V}^{\text{V}}\text{O}(\text{OMe})]^{2+}$ complexes catalyzed the Hantzsch reaction under the above conditions to give only two different products: (a) diethyl 2,6-dimethyl-4-phenyl-1,4-dihydropyridine-3,5-dicarboxylate (1,4-DHP) and (b) diethyl 2,6-dimethyl-4-phenylpyridine-3,5-dicarboxylate (Py). An initial screening using complex **1** as a representative catalyst also resulted in the formation of the same two major products.

<<Scheme 3>>

The experimental reaction conditions were optimized considering various parameters, like amounts of oxidant, solvent, catalyst and temperature. Thus, for a mixture of 0.005 mol (0.53 g) of benzaldehyde, 0.010 mol (1.30 g) of ethyl acetoacetate and 0.005 mol (0.38 g) of ammonium acetate in a reaction flask, three different amounts of catalyst **1** [0.001 g (1×10^{-3} mmol), 0.002 g (2×10^{-3} mmol) and 0.003 g (3×10^{-3} mmol)] and aqueous 30% H_2O_2 (0.005 , 0.010 and 0.015 mol) were added and the reaction was run at four different temperatures (30 , 40 , 50 and 60 °C). Details

for all these conditions, the conversion and selectivity of the different products under particular conditions are summarized in Table 6 (Fig. S13).

<<Table 6>>

It is clear from the data in Table 6 that the optimized reaction conditions to achieve the maximum conversion (with respect to 1,4-DHP) in 1 h of reaction time are (entry 6): catalyst **1** (0.001 g, 1×10^{-3} mmol) and H₂O₂ (0.560 g, 0.005 mol) at 30 °C, where a maximum 88% conversion along with 100% selectivity of dihydropyridine was achieved under solvent free reaction conditions. These products were also identified by HRMS (Figs. S14-S16), as well as by ¹H NMR spectroscopy (after separating them by column chromatography) (Fig. S17). Increasing the temperature to 40 °C increases the conversion, but the selectivity of product (a) drops slightly (entry 7). The conversion as well as the selectivity drop on further increasing the temperature. Increasing the oxidant has the least effect on the conversion. The effect of different solvents, like MeOH, EtOH, CH₂Cl₂, CHCl₃, MeCN, DMSO and hexane, have also been studied under the optimized reaction conditions (i.e. entry 6 of Table 6) and the conversion with respect to the solvents follows the order: MeOH (90%) > EtOH (87%) > MeCN (85%) > CH₂Cl₂ (82%) > CHCl₃ (78%) > hexane (72%) > DMSO (23%) (entries 9 to 16 of Table 6). The blank runs (i.e. without catalyst) with solvents are given in Table S4 (see also entries 17 to 22 of Table 6), which conclude that there is no significant role of the solvent to drive the reaction. Thus, the reactions in solvents, except MeOH, have no added benefit in terms of conversion. However, if importance is given to the aromatized product, the reactions in solvents do result in an improved selectivity of the aromatized product (b) and a decrease in the selectivity of product (a). Thus, within the range of solvents used, non-polar solvents show better selectivity for product (b).

3.8. Scope of the reaction

We have further explored the scope of this reaction using all the complexes as catalysts while taking different derivatives of benzaldehyde and examined the yield of the obtained reaction products along with conversion after different time intervals under the optimized reaction conditions. It was observed that (i) introduction of an electron withdrawing group (–NO₂, –Cl or –F groups) yielded the maximum conversion 94-98 % while an electron donating group (–CH₃ or –OMe) gave a lower conversion 82-87% (Table S5). Thus, after the first 1 h of reaction, the overall

conversion for different substituents of benzaldehyde followed the order: $\text{NO}_2 > \text{F} > \text{Cl} > \text{H} > \text{CH}_3 > \text{OMe}$, (ii) complex **3** is the best amongst all complexes, though all of them show very good catalytic activity, (iii) the time analysis suggests that all the complexes result in the formation of the dihydropyridine derivative (a) selectively at 30 °C in the first 1 h of the reaction and then the conversion of dihydropyridine to the pyridine derivatives starts and complete conversion occurs in ca. 10 h (Fig. 6) and (iv) a change in color of the reaction product can also be visualized (Fig. 6(A)).

<<Figure 6>>

For a systematic comparison of the catalytic activity of the trinuclear dioxidomolybdenum(VI) complexes with the analogous mono- and dinuclear-dioxidomolybdenum(VI) complexes, we have conducted the catalytic experiment considering the same molybdenum content of each catalyst as considered for the trinuclear system. It was found that the mononuclear complex $\text{H}_4\text{ptk-bhz}$ (the Schiff base obtained from equimolar amounts of 2, 4, 6-trihydroxybenzene-1, 3, 5-tricarbaldehyde and benzoylhydrazide) gives 22% conversion with 8% selectivity of (a), while the dinuclear analogue ($\text{H}_4\text{dar-inh}$ = Schiff base obtained from one equivalent of 4, 6-dihydroxyisophthalaldehyde and two equivalents of isonicotinoylhydrazide) gives 34% conversion with 12% selectivity of (a) within 1 h of reaction time. Interestingly, the complete conversion of the reactants into product and the reversal of the selectivity of the product after about 10 h of reaction time increase the scope of the complexes considered here as catalysts for these multicomponent reactions

3.9. Possible reaction mechanism for the Hantzsch reaction

3.9.1. UV-visible spectroscopic study

Aiming towards understanding the possible mechanistic pathways for the multi component Hantzsch reaction we have conducted a series of experiments, whose descriptions are given below. (i) As a representative example, a methanolic solution of complex **1** was treated with H_2O_2 and the resulting changes were monitored by UV-visible spectroscopy. Thus, treatment of 25 ml of **1** (4×10^{-5} M) in MeOH with one drop portions of 30 % H_2O_2 dissolved in 10 mL of MeOH (the final concentration of the H_2O_2 solution is ca. 9.0×10^{-2} M) causes the splitting of a broad band appearing at ca. 325 nm into two with an increase in their intensity. The intensity of the first band at 220 nm slowly increases, while the second band further splits into two (288 and 331 nm) along

with an increase in intensity. Based on their intensity, these bands are $n \rightarrow \pi^*$ and the split bands are $\pi - \pi^*$, respectively [Fig. S18(a)]. Simultaneously, the intensity of the LMCT band also reduces and finally it becomes almost flat. The other complexes show very similar spectral changes upon addition of H_2O_2 , except **7** (Figs. S19-S24).

(ii) We have also carried out the above reaction in DMSO and the spectral changes are presented in Fig. S18(b) and Figs. S25-S30. In DMSO, the addition of H_2O_2 causes a reduction in the intensity of the LMCT band at 412 nm, followed by its flattening, while the band at 321 nm usually splits into two bands (in complexes **1**, **5** and **6**), one at higher wavelength and other one at a lower wavelength along with a slight decrease in intensity, as observed in MeOH. In complexes **2**, **3** and **7**, this band shifts towards the higher wavelength, along with a slight decrease in intensity. Only the band at ca. 260 nm gains in intensity. These spectral changes finally led to the generation of at least one isosbestic point at ca. 360 nm, or in some cases two (ca. 360 and ca. 300 nm). These observations hint towards the interaction of the peroxide ion with the complexes and the generation of the corresponding oxidoperoxidomolybdenum(VI) species in solution. In the case of **7**, three isobestic points were observed at 409, 371 and 312 nm.

(iii) The systematic addition of one drop portions of benzaldehyde in 10 mL of MeOH (the final concentration of the benzaldehyde solution is 9.4×10^{-2} M) to the final reaction mixture obtained after adding H_2O_2 to **1** in MeOH (see Fig. S18(c)) causes a considerable increase in the intensity of the 280 and 333 nm bands without altering their positions, while the original band at ca. 410 nm, which disappeared during the peroxido species generation, starts gaining intensity with a slight shift towards a higher wavelength. Simultaneously, the other two bands i.e. the 225 and 360 nm bands, gain considerable and marginal increments in intensity, respectively. Successive addition of one drop portions of an ethyl acetoacetate (7.7×10^{-4} M) solution in MeOH to the above solution also indicates its interaction with the intermediate species formed [Fig. S18(d)] as the $n \rightarrow \pi^*$ and split $\pi - \pi^*$ bands show further visible changes in their intensity.

(iv) A solution of 25 ml of **1** (4×10^{-5} M) in MeOH was titrated with the successive addition of one drop portions of benzaldehyde (9.4×10^{-2} M) in MeOH and the resulting spectroscopic changes are depicted in Fig. S31(a). Thus, the intensities of the UV band at 318 nm and LMCT band at 420 nm improve with no change in their positions, while the 257 nm band shifts to a higher wavelength with a considerable increase in intensity. Additionally, a new band at 280 nm starts appearing, suggesting the interaction of benzaldehyde with the metal center. The intensities of all the bands

(except that at 420 nm) further increase upon addition of a methanolic solution of H₂O₂ (9×10^{-2} M) to the above solution of complex **1**, while the LMCT band shows the opposite trend, i.e. decreases with the addition of H₂O₂ [Fig. S31(b)]. Interestingly, a weak band at ca. 310 nm is also generated along with the appearance of an isosbestic point at 375 nm. These observations are in line with the interaction of H₂O₂ with the benzaldehyde interacted complex **1**. The intensity of the 420 nm band remains constant while all the other bands show a positive change in intensity, which further show its positive effect on the surroundings of the metal center [Fig. S31(c)].

3.9.2. A DFT investigation

Density functional theory (DFT) computations were performed to explore the possible intermediates present in the reaction. In order to do that, we constructed mononuclear and trinuclear based computational model systems. The optimized structures deduced planar geometries of the complexes (see Fig. 7). So as to reduce the computational time, the mononuclear computational model is preferred.

We have studied two pathways (**I** and **II**) commencing from **1(A)** (a mononuclear unit of **1**) which lead to the intermediate **1(D)**. The two pathways differ in their order of addition of benzaldehyde and H₂O₂. In path-**I**, benzaldehyde is added first whereas in path-**II**, H₂O₂ is mixed with **1(A)** in the first step.

<<Figure 7>>

In path-**I**, the reaction starts by the addition of benzaldehyde, which replaces the water molecule present at the axial position of the molybdenum center. This addition leads to the formation of the complex intermediate **1(B)**. Interestingly, we see a stabilization energy of 1.5 kcal mol⁻¹ after the binding of benzaldehyde at the molybdenum center (Fig. 8). This stabilization energy is due to the π - π stacking, as seen in the figure. Following path-**1**, in the second step, H₂O₂ is added to intermediate **1(B)**, which however destabilizes intermediate **1(BD)** as the benzaldehyde leaves the axial position, and thus the π - π stacking is lost. Intermediate **1(BD)** is significantly stabilized by ~ 9 kcal mol⁻¹ to yield the intermediate **1(D)** by eliminating a water molecule; in this process benzaldehyde recombines at the axial position to build the π - π stacking once again. However, no covalent bonding exists between the molybdenum center and the oxygen center of the benzaldehyde ($d(\text{Mo}-\text{O}) = 2.5 \text{ \AA}$), See Fig. 8. Hence, the DFT investigation of path-**I** clearly shows that the addition of benzaldehyde builds the π - π stacking interaction in the initial and the

final steps of the pathway. Such an interaction helps in stabilizing the reaction intermediates **1(B)** and **1(D)**.

In path-**II**, H₂O₂ is added in the first step and benzaldehyde is mixed in the last. Clearly, after the addition of H₂O₂ to **1(A)** we did not observe any stabilization as the intermediate **1(AC)** is destabilized by 6 kcal mol⁻¹ relative to **1(A)**. However, the intermediate **1(AC)** is significantly stabilized by ~20 kcal mol⁻¹ after the elimination of a water molecule. In the final step, benzaldehyde is reacted with intermediate **1(AC)**, but to our surprise it was found that intermediate **1(C)** is still more stable than intermediate **1(D)**. Based on our DFT study, we therefore propose that the reaction mixture will have both intermediate **1(C)** and intermediate **1(D)**, but with a slight dominance of intermediate **1(C)**.

We have also studied the addition of methyl acetoacetate (MAA) with **1(D)** as well as with **1(B)** (see Fig. 8). In case of **1(D)** reacting with MAA, the intermediate **1(DC)** forms showing the formation of a C-C bond. The intermediate **1(DC)** is relatively more stable than **1(D)** by 11.3 kcal mol⁻¹, which justifies the formation of **1(DC)** via **1(D)**. Reaction of **1(B)** with MAA gives rise to **1(BA)**, in which C-C bond formation takes place as seen in **1(DC)**. The intermediate **1(DC)** is found to be ~7 kcal mol⁻¹ more stable than **1(BA)**. So, the relative stability of **1(BA)** as compared to **1(DC)** suggests that the later one is preferred to yield **Int1** but note the route through **1(BA)** cannot be ignored. Now, **Int1** and **Int2** undergo a cyclization reaction to yield **P1**, which reacts with **1(C)** and forms the aromatic product **P2** with the complex **1(CA)**. The complex **1(CA)**, which is the highest stable intermediate in the catalytic cycle, gives rise to the starting complex **1(A)** by the removal of a water molecule.

<<Figure 8>>

Since the actual ligand **I** has three ligating units at the 1, 3 and 5 positions on the benzene ring, the possibility of the existence of mono-, di- and trinuclear *cis*-[MoO₂]²⁺ complexes also exists. Therefore, we have also tried to see through a computational study if these mono-, di- and trinuclear *cis*-[MoO₂]²⁺ complexes are stable and produce the corresponding stable peroxido complexes as well. In fact, for the mononuclear case, the peroxido species **9** is stabilized by ~8.0 kcal mol⁻¹ compared to mononuclear complex **8**. Similarly, the dinuclear peroxido system **11** is ~15.0 kcal mol⁻¹ more stable than the dinuclear dioxido complex **10**, whilst the trinuclear peroxido complex (**12**) is stabilized by ~23.0 kcal mol⁻¹ relative to the trinuclear dioxide complex **1**. These

studies clearly show that as we move from mono- to di- and then to tri-nuclear complexes, the relative stability of the corresponding peroxido complex increases with respect to its corresponding dioxido complex (Figs. S32–34).

Based on the DFT studies, a suitable reaction mechanism has been proposed, as shown within Fig. 8, where the *cis*-[MoO₂]²⁺ complex interacts first with H₂O₂ to form its peroxido intermediate followed by its interaction with benzaldehyde, which in turn reacts with ethyl acetoacetate to provide intermediate - I. Formation of intermediate - II by the reaction of ammonium acetate and ethyl acetoacetate is obvious. Finally, both intermediates react together to give DHP. This DHP undergoes aromatization in the presence of the peroxido species to give the corresponding pyridine and original dioxido complex.

4. Conclusions

We have prepared tris[*cis*-MoO₂]²⁺-complexes, [{Mo^{VI}O₂(MeOH)}₃L¹⁻⁷] (**1–7**), with trinucleating ligands derived from benzene-1,3,5-tricarbohydrazide and salicylaldehyde derivatives. A single crystal X-ray study confirms the six-coordinated distorted octahedral geometry around each Mo center and the overall structure adopts a high C₃-symmetry with a phenyl group in the center and three arms. DFT calculations endorse the stabilization of their peroxido derivatives (e.g. [{Mo^{VI}O(O₂)(H₂O)}₃L¹] (**12**)) as well. The trinuclear complex **12** has $\Delta H = -23.4$ kcal mol⁻¹, while the binuclear and mononuclear oxidoperoxido molybdenum(VI) complexes have relatively lower ΔH values. Cyclic voltammetry data, in support of differential pulse voltammetry data, are in conformity with the irreversible redox behaviour in DMF. The high catalytic efficiency of these complexes towards the one pot Hantzsch reaction of three components involving ethyl acetoacetate, benzaldehyde (or its derivatives) and ammonium acetate in solvent and solvent free systems has shown very interesting results in that the initial 1 h of the catalytic reaction produces dihydropyridine selectivity along with a high TOF value, but with the elapse of time the dihydropyridine derivative slowly changes to the pyridine derivative and finally the reaction becomes selective for the pyridine derivative after about 10 h. A DFT study provides all the probable intermediates present in the catalytic reaction. This method provides excellent selectivity between the products, involving easy workup with excellent yields. This method can be extended for the synthesis of important hetero-nuclei compounds to develop pharmaceutical drugs.

Appendix A. Supplementary data

CCDC 1952306 for complex **1a**, 1952307 for **5a** and 1952308 for ligand **IIIa** contain the supplementary crystallographic data for the structures. These data can be obtained free of charge via <http://www.ccdc.cam.ac.uk/conts/retrieving.html>, or from the Cambridge Crystallographic Data Centre, 12 Union Road, Cambridge CB2 1EZ, UK; fax: (+44) 1223 336 033; or e-mail: deposit@ccdc.cam.ac.uk.

Acknowledgements

MRM thanks the Science and Engineering Research Board (SERB), Government of India, New Delhi, for financial support of the work (grant number CRG/2018/000182). PG acknowledges the Faculty Initiation Grant (FIG–100810) and computational facilities provided by IIT Roorkee. RT is thankful to the Indian Institute of Technology (IIT) Roorkee, India, for the Institute fellowship

Conflicts of Interest

Authors declare no conflict of interest.

References

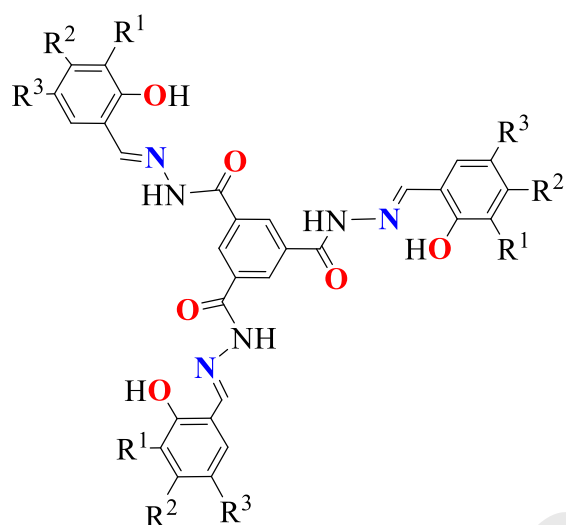
1. (a) M. Amini, M. M. Haghdoost, M. Bagherzadeh, *Coord. Chem. Rev.* 257 (2013) 1093-1121; (b) K. Heinze, *Coord. Chem. Rev.* 300, (2015) 121-141; (c) J. C. Pessoa, I. Correia, *Coord. Chem. Rev.* 388 (2019) 227-247.
2. (a) D. Cvijanović, J. Pisk, G. Pavlović, D. Šišak-Jung, D. M. Čalogović, M. Cindrić, D. Agustin, V. Vrdoljak, *New J. Chem.* 43 (2019) 1791-1802; (b) K. Uzarevic, G. Pavlovic, M. Cindrić, *Polyhedron* 52 (2013) 294-300.
3. (a) M. K. Hossain, J. A. Schachner, M. Haukka, N. C. Mosch-Zanetti, E. Nordlander, A. Lehtonen, *Inorg. Chim. Acta* 486 (2019) 17-25; (b) D. Cvijanović, J. Pisk, G. Pavlović, D. Šišak-Jung, D. Matković-Čalogović, M. Cindrić, D. Agustin, V. Vrdoljak, *New J. Chem.* 43 (2019) 1791-1802; (c) P. Neves, S. Gago, S. S. Balula, A. D. Lopes, A. A. Valente, L. Cunha-Silva, F. A. A. Paz, M. Pillinger, J. Rocha, C. M. Silva, I. S. Gonçalves, *Inorg. Chem.* 50 (2011) 3490-3500; (d) N. Zwettler, J.A. Schachner, F. Belaj, N.C. Mösche-Zanetti, *J Mol. Catal. A:*

- Chem. 443 (2017) 209-219; (e) M. R. Maurya, L. Rana, N. Jangra, F. Avecilla, Chemistry Select 2 (2017) 6767-6777.
- M. R. Maurya, R. Tomar, L. Rana, F. Avecilla, Eur. J. Inorg. Chem. (2018) 2952-2964.
 - (a) F. Bossert, H. Meyer, E. Wehinger, Angew. Chem. Int. Ed. Engl. 20 (1981) 762-769; (b) B. Love, M. M. Goodman, K. M. Snader, R. Tedeschi, E. Macko, J. Med. Chem. 17 (1974) 956-965; (c) P. K. Gilpin, L. A. Pachla, Anal. Chem. 71 (1999) 217-233; (d) S. Cosconati, L. Marinelli, A. Lavecchia, E. Novellino, J. Med. Chem. 50 (2007) 1504-1513.
 - (a) J. W. Yang, M. T. H. Fonseca, B. List, Angew. Chem. Int. Ed. Eng. 436 (2004) 6660-6662; (b) S. G. Ouellet, J. B. Tuttle, D. W. C. MacMillan, J. Am. Chem. Soc. 127 (2005) 32-33; (c) J. W. Yang, M. T. H. Fonseca, N. Vignola, B. List, Angew. Chem. Int. Ed. Eng. 44 (2005) 108-110.
 - Z. Liu, Q. Liu, W. Zhang, R. Mu, L. Yang, Z-L Liu, W. Yu, Chem. Inform. 5 (2006) 771-734.
 - Z. Liu, B. Han, Q. Liu, W. Zhang, L. Yang, Z- L. Liu, W. Yu, Synlett. 10 (2005) 1579-1580.
 - (a) S. Hoffmann, N. Nicoletti, B. List, J. Am. Chem. Soc. 128 (2006) 13074-13075; (b) Z. Zhang, P. R. Schreiner, Synlett. 9 (2007) 1455-1457.
 - M. Rueping, T. Theissmann, A. P. Antonchick, Synlett. 7 (2006) 1071-1074.
 - X-Q. Zhu, H-Y Wang, Wang J-S, Y-C. Liu, J. Org. Chem. 66 (2001) 344-347.
 - (a) Y. Xia, H. Huang, F. Zhang, G. Deng, Org. Lett. 21 (2019) 7489-7492; (b) T. Momeni, M. M. Heravi, T. Hosseinejad, M. Mirzaei, V. Zadsirjan, J. Mol. Struct. 1199 (2020) 127011; (c) M. Gupta, D. De, K. Tomar, P. K. Bhardwaj, Inorg. Chim. Acta, 482 (2018) 925-934; (d) C. G. Evans, J. E. Gestwicki, Org. Lett. 11 (2009) 2957-2959; (e) S. Wang, H. Chen, H. Zhao, H. Cao, Y. Li, Q. Liu, Eur. J. Org. Chem. (2013) 7300-7304; (f) M. F. Litvić, M. Litvić, V. Vinkovic, Tetrahedron 64 (2008) 10912-10918; (g) N. Jagadishbabu, K. Shivashankar, RSC Adv. 5 (2015) 95240-95246.
 - K. Niknam, M. A. Zolfigol, S. M. Razavian, B. I. Mohammadpoor, J. Heterocycl. Chem. 43 (2006) 199-202.
 - G. Sabitha, K. K. Reddy, G. S. Reddy, N. Fatima, J. S. Yadav, Synthesis 8 (2003) 1267-1271.
 - K. J. Ko, J. Y. Kim, Tetrahedron Lett. 40 (1999) 3207-3208.
 - C. G. Evans, J. E. Gestwicki, Org. Lett. 14 (2009) 2957-2959.
 - O. Garcia, F. Delgado, A. C. Cano, C. Alvarez, Tetrahedron Lett. 34 (1993) 623-625.

18. M. M. Heravi, F. S. S. Moosavi, Y. S. Beheshtiha, M. Ghassemzadeh, *Heterocycl Commun.* 10 (2004) 415-418.
19. J. J. E. Vanden, F. Delfaese, A. Mayence, Y. V. Haverbeke, *Tetrahedron* 51 (1995) 6511-6516.
20. C. Alvarez, F. Delgado, O. Garcia, S. Medina, C. Marquez, *Synth. Commun.* 21 (1991) 619-624.
21. J. J. Xia, Wang, *Synthesis* 14 (2005) 2379-2383.
22. J. W. Lee, K. Y. Ko, *Bull. Korean Chem. Soc.* 25 (2004) 19-20.
23. J. Arguello, L. J. N. Vergara, J. C. Sturm, J. A. Suuella, *Electrochim. Acta* 49 (2004) 4849-4856.
24. M. M. Heravi, F. Dirkwand, H. A. Oskooie, M. Ghassemzadeh, *Heterocycl Commun.* 11 (2005) 75-78.
25. A. Saini, S. Kumar, J. S. Sandhu, *Synth. Commun.* 37 (2007) 2317-2324.
26. P. Sharma, M. Gupta, *Green Chem.* 17 (2015) 1100-1106.
27. M. R. Maurya, N. Saini, F. Avecilla, *RSC Adv.* 6 (2016) 12993-13009.
28. M. R. Maurya, B. Sarkar, F. Avecilla, I. Correia, *Dalton Trans.* 45 (2016) 17343-17364.
29. M. Nasr-Esfahani, M. Moghadam, G. Valipour, *Synth. Commun.* 39 (2009) 3867-3879.
30. M. Filipan-Litvić, M. Litvić, I. Capanec, V. Vinkovi, *ARKIVOC* (2008) 96-103.
31. M. Litvić, M. Regović, K. Šmic, M. Lovrić, M. Filipan-Litvić, *Bioorg. Med. Chem. Lett.* 22 (2012) 3676-3681.
32. R. Surasani, D. Kalita, A.V.D. Rao, K. Yarbagi, K.B. Chandrasekhar, *J. F. Chem.* 135 (2012) 91-96.
33. S. H. Mashraqui, M. A. Karnik, *Tetrahedron Lett.* 39 (1998) 4896-4898.
34. M. M. Hashemi, Y. Ahmadibeni, H. Ghafuri, *Monatsh. Chem.* 134 (2003) 107-110.
35. S. Xu, L. Liu, Y. Wang, *Sep. Purification Technology* 185 (2017), 215-226.
36. G. J. J. Chen, J. W. McDonald, W. E. Newton, *Inorg. Chem.* 15 (1976) 2612-2615.
37. G. M. Sheldrick, *SADABS*, Version 2.10, University of Göttingen, Germany (2004).
38. G. M. Sheldrick, *SHELX*, *Acta Crystallogr. Sect. C.* 71 (2015) 3-8.
39. F. Neese, *WIREs Comput. Mol. Sci.* 2 (2012) 73-78.

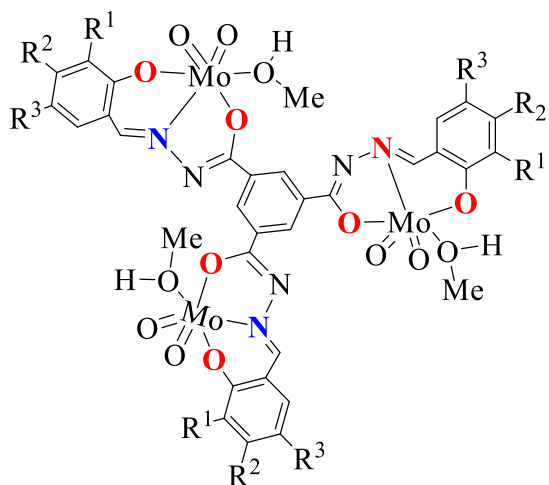
40. (a) A. D. Becke, *Phys. Rev. A: At., Mol., Opt. Phys.* 38 (1988) 3098-3100; (b) A. D. J. Becke, *Chem. Phys.* 98 (1993) 5648-5652; (c) C. Lee, W. Yang, R. G. Parr, *Phys. Rev. B: Condens. Matter Mater. Phys.* 37 (1988) 785-789.
41. A. Schäfer, C. Huber, R. Ahlrichs, *J. Chem. Phys.* 100 (1994) 5829-5835.
42. F. Neese, F. Wennmohs, A. Hansen, U. Becker, *Chem. Phys.* 356 (2009) 98-109.
43. S. Grimme, S. Ehrlich, L. Goerigk, *J. Comput. Chem.* 32 (2011) 1456-1465.
44. (a) A. Syamal, M. R. Maurya, *Coord. Chem. Rev.* 95 (1989) 183-238; (b) R. Dinda, P. Sengupta, S. Ghosh, H. M. Figge, W. S. Sheldrick, *J. Chem. Soc., Dalton Trans.* 23 (2002) 4434-4439.
45. (a) S. Pasayat, S. P. Dash, S. Majumder, R. Dinda, E. Sinn, H. S. Evans, S. Mukhopadhyay, S. K. Bhutia, P. Mitra, *Polyhedron* 80 (2014) 198-205; (b) S. Majumder, S. Pasayat, A. K. Panda, S. P. Dash, S. Roy, A. Biswas, M. E. Varma, B. N. Joshi, E. Garribba, C. Kausar, S. K. Patra, W. Kaminsky, A. Crochet, R. Dinda, *Inorg. Chem.* 56 (2017) 11190-11210.
46. R. Dinda, P. Sengupta, S. Ghosh, H. M. Figge, W. S. Sheldrick, *J. Chem. Soc., Dalton Trans.* 23 (2002) 4434-4439.
47. M. Chaudhary, *J. Chem. Soc., Dalton Trans.* 2 (1984) 115-120.
48. (a) O. D'Alessandro, Á. G. Sathicq, J. E. Sambeth, H. J. Thomas, G. P. Romanelli, *Catal. Commun.* 60 (2015) 65-69; (b) L. Shen, S. Cao, J. Wu, J. Zhang, H. Li, N. Liu, X. Qian, *Green Chem.* 11 (2009), 1414-1420.

Schemes



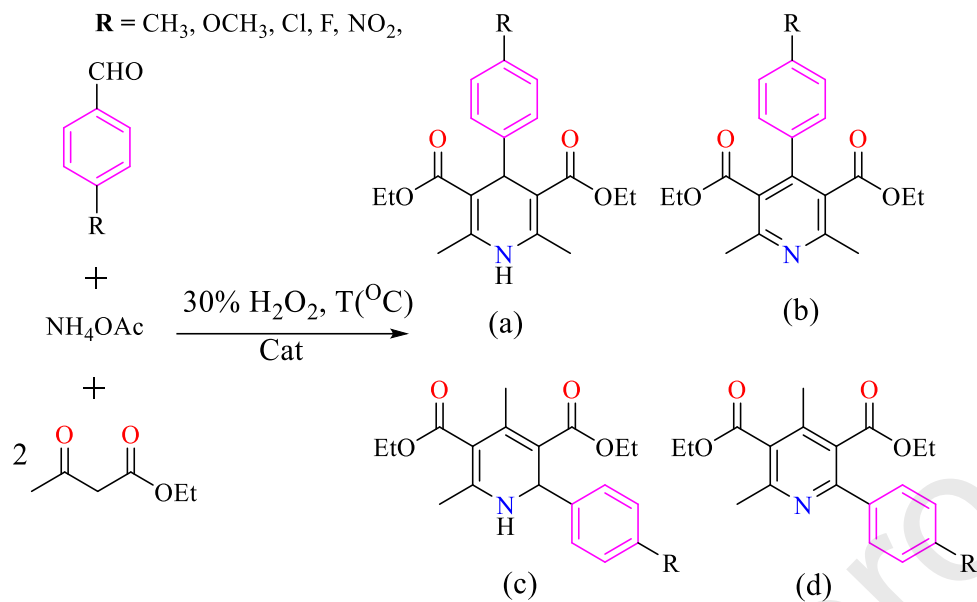
$R^1=H, R^2=H, R^3=H$	H_6L^1 (I)
$R^1=C(CH_3)_3, R^2=H, R^3=C(CH_3)_3$	H_6L^2 (II)
$R^1=H, R^2=OMe, R^3=H$	H_6L^3 (III)
$R^1=OH, R^2=H, R^3=H$	H_6L^4 (IV)
$R^1=H, R^2=Cl, R^3=H$	H_6L^5 (V)
$R^1=H, R^2=Me, R^3=H$	H_6L^6 (VI)
$R^1=H, R^2=N(CH_2CH_3)_2, R^3=H$	H_6L^7 (VII)

Scheme 1. Trinucleating ligands, designated as **I-VII**, used in this work.



- $R^1=H, R^2=H, R^3=H$ $[\{MoO_2(MeOH)\}_3L^1]$ (1)
 $R^1=C(CH_3)_3, R^2=H, R^3=C(CH_3)_3$ $[\{MoO_2(MeOH)\}_3L^2]$ (2)
 $R^1=H, R^2=OMe, R^3=H$ $[\{MoO_2(MeOH)\}_3L^3]$ (3)
 $R^1=OH, R^2=H, R^3=H$ $[\{MoO_2(MeOH)\}_3L^4]$ (4)
 $R^1=H, R^2=Cl, R^3=H$ $[\{MoO_2(MeOH)\}_3L^5]$ (5)
 $R^1=H, R^2=Me, R^3=H$ $[\{MoO_2(MeOH)\}_3L^6]$ (6)
 $R^1=H, R^2=N(CH_2CH_3)_2, R^3=H$ $[\{MoO_2(MeOH)\}_3L^7]$ (7)

Scheme 2. Proposed structure of the dioxidomolybdenum(VI) complexes.



Scheme 3. Four expected products of the Hantzsch reaction using reactants benzaldehyde, ethyl acetoacetate and ammonium acetate: (a) diethyl 2,6-dimethyl-4-phenyl-1,4-hydropyridine-3,5-dicarboxylate, (b) diethyl 2,6-dimethyl-4-phenylpyridine-3,5-dicarboxylate, (c) diethyl 2,4-dimethyl-6-phenyl-1,4-dihydropyridine-3,5-dicarboxylate and (d) diethyl 2,4-dimethyl-6-phenylpyridine-3,5-dicarboxylate.

Tables

Table 1

Crystal data and structure refinement for the compounds [$\{\text{MoO}_2(\text{DMSO})\}_3\text{bthz}(\text{sal})_3$] (**1a**), [$\{\text{MoO}_2(0.5\text{H}_2\text{O}\cdot 0.5\text{MeOH})\}\{\text{MoO}_2(\text{DMF})\}\{\text{MoO}_2(\text{DMSO})\}_3\text{bthz}(\text{Cl-sal})_3\cdot \text{DMF}\cdot 0.5\text{DMSO}$] (**5a**) and $\text{H}_6\text{bthz}(\text{MeO-sal})_3\cdot 3\text{DMF}$ (**IIIa**).

	1a	5a	IIIa
Formula	$\text{C}_{36}\text{H}_{38}\text{Mo}_3\text{N}_6\text{O}_{18}\text{S}_3$	$\text{C}_{39.50}\text{H}_{40}\text{Cl}_3\text{Mo}_3\text{N}_8\text{O}_{16.50}\text{S}_{1.50}$	$\text{C}_{42}\text{H}_{50}\text{N}_9\text{O}_{12}$
Formula weight	1176.71	1333.06	872.91
T, K	100(2)	100(2)	100(2)
Wavelength, Å	0.71073	0.71073	0.71073
Crystal system	Hexagonal	Triclinic	Orthorhombic
Space group	$R\bar{3}$	$P\bar{1}$	$P2_12_12_1$
<i>a</i> , Å	20.4234(14)	10.3331(8)	4.9394(2)
<i>b</i> , Å	20.4234(14)	15.2717(12)	25.3279(10)
<i>c</i> , Å	21.1588(15)	18.3593(14)	34.4133(14)
α , °	90	96.946(3)	90
β , °	90	90.455(3)	90
γ , °	120	99.565(3)	90
<i>V</i> , Å ³	7643.2(9)	2834.8(4)	4305.3(3)
<i>Z</i>	6	2	4
<i>F</i> ₀₀₀	3528	1332	1844
<i>D</i> _{calc} , g cm ⁻³	1.534	1.562	1.347
μ , mm ⁻¹	0.914	0.917	0.100
θ , °	2.89 to 27.15	1.65 to 26.42	2.37 to 26.42
<i>R</i> _{int}	0.0380	0.1009	0.0639
Crystal size, mm ³	0.26 × 0.24 × 0.19	0.04 × 0.15 × 0.22	0.29 × 0.18 × 0.17
Goodness-of-fit on <i>F</i> ²	1.099	1.076	1.066
<i>R</i> ₁ [<i>I</i> > 2σ(<i>I</i>)] ^a	0.0662	0.0827	0.0538
<i>wR</i> ₂ (all data) ^b	0.2029	0.2894	0.1569
Largest differences peak and hole, e Å ⁻³	4.248 and -1.013	1.706 and -1.229	0.834 and -0.267

$$^a R_1 = \frac{\sum ||F_o| - |F_c||}{\sum |F_o|} \quad ^b wR_2 = \left\{ \frac{\sum [w(|F_o|^2 - |F_c|^2)|^2]}{\sum [w(F_o^2)^2]} \right\}^{1/2}$$

Table 2

Bond lengths [Å] and angles [°] for the compounds [$\{\text{MoO}_2(\text{DMSO})\}_3\text{bthz}(\text{sal})_3$] (**1a**), [$\{\text{MoO}_2(0.5\text{H}_2\text{O}\cdot 0.5\text{MeOH})\}\{\text{MoO}_2(\text{DMF})\}\{\text{MoO}_2(\text{DMSO})\}\text{bthz}(\text{Cl-sal})_3\cdot \text{DMF}\cdot 0.5\text{DMSO}$] (**5a**) and $\text{H}_6\text{bthz}(\text{MeO-sal})_3\cdot 3\text{DMF}$ (**IIIa**).

Bond lengths	1a	5a	IIIa
Mo(1)-O(1)	1.710(4)	1.697(7)	
Mo(1)-O(2)	1.694(5)	1.686(7)	
Mo(1)-O(3)	2.000(4)	1.931(7)	
Mo(1)-O(4)	1.930(4)	2.003(6)	
Mo(1)-N(1)	2.247(5)	2.251(8)	
Mo(1)-O(1M)	2.220(6)	Mo(1)-O(1WA) 2.298(9)	
N(1)-N(2)	1.403(6)	1.407(9)	1.384(3)
N(3)-N(4)			1.370(3)
N(5)-N(6)			1.369(3)
O(3)-C(3)	1.315(7)	O(3)-C(14) 1.348(12)	
O(1)-C(7)			1.231(3)
O(4)-C(16)			1.223(3)
O(7)-C(25)			1.224(3)
Angles	1a	5a	IIIa
O(2)-Mo(1)-O(1)	104.0(3)	103.8(4)	
O(2)-Mo(1)-O(3)	97.5(3)	99.0(3)	
O(1)-Mo(1)-O(3)	97.96(19)	101.7(3)	
O(2)-Mo(1)-O(4)	97.5(3)	95.2(3)	
O(1)-Mo(1)-O(4)	104.1(2)	98.6(3)	
O(3)-Mo(1)-O(4)	149.57(19)	151.7(3)	
O(2)-Mo(1)-N(1)	89.48(18)	94.8(3)	
O(1)-Mo(1)-N(1)	164.38(19)	160.0(4)	
O(3)-Mo(1)-N(1)	71.78(13)	82.2(3)	
O(4)-Mo(1)-N(1)	81.86(17)	72.2(3)	
O(2)-Mo(1)-O(1M)	170.7(2)		

O(1)-Mo(1)-O(1M)	84.9(3)	
O(4)-Mo(1)-O(1M)	82.9(2)	
O(3)-Mo(1)-O(1M)	78.4(2)	
O(1)-C(7)-N(1)		123.0(3)
O(1)-C(7)-C(1)		121.0(2)
O(4)-C(16)-N(3)		121.5(2)
O(4)-C(16)-C(5)		121.8(2)
O(7)-C(25)-N(5)		121.9(3)
O(7)-C(25)-C(3)		121.2(2)

Table 3Hydrogen bonds in the compound H₆bthz(MeO-sal)₃·3DMF (**IIIa**).

D-H...A	d(D-H), Å	d(H...A), Å	d(D...A), Å	<(DHA), °
N(1)-H(1N)...O(2D)	0.86(4)	2.02(4)	2.858(3)	167(3)
O(2)-H(2)...N(2)	0.82	1.89	2.607(3)	145.0
N(3)-H(3N)...O(3D)#1	0.90(4)	1.93(5)	2.812(3)	168(4)
O(5)-H(5)...N(4)	0.82	1.88	2.599(3)	145.7
N(5)-H(5N)...O(1D)	0.80(3)	2.09(3)	2.880(3)	167(3)
O(8)-H(8)...N(6)	0.82	1.87	2.593(3)	145.5

Symmetry transformations used to generate equivalent atoms: #1 x-1,y,z

Table 4.¹H NMR (400 MHz) data (δ in ppm) of the ligands and the complexes.

Comp.	-OH	-NH	-CH=N	Ar-H	-OH	-OMe (methanolic)	Methyl protons
I	11.16 (br, 3H)	12.44 (s, 3H)	8.73 (s, 3H)	6.91 (t, J=7.8 Hz, 6H), 7.29 (t, J=8.6 Hz, 3H), 7.58 (d, J=7.8 Hz, 3H), 8.72 (s, 3H)	---	---	---
1	---	---	9.15 (s, 3H)	6.96 (t, J=8.3 Hz, 3H), 7.10 (t, J=7.1 Hz, 3H), 7.55 (t, J=7.8 Hz, 3H), 7.73 (d, J=9.4 Hz, 3H), 8.75 (s, 3H),	4.04 (br, 3H)	3.12 (s, 9H)	---
II	12.61 (br, 3H)	12.22 (s, 3H)	9.85 (s, 3H)	7.24 (s, 3H), 7.26 (s, 3H), 7.35 (s, 3H), 8.70 (s, 3H)	---	---	1.44 (s, 9H), 1.30 (s, 9H)
2	---	---	9.19 (s, 3H)	7.29 (s, 3H), 7.56 (s, 3H), 7.68 (s, 3H), 8.79 (s, 3H)	4.13 (br, 3H)	3.17 (s, 9H)	1.38 (s, 9H), 1.32 (s, 9H)
III	10.77 (br, 3H)	12.36 (s, 3H)	8.71 (s, 3H)	6.85 (t, J=7.9 Hz, 3H), 7.03 (d, J=7.5 Hz, 3H), 7.18 (d, J=7.4 Hz, 3H), 8.69 (s, 3H)	---	---	3.79 (s, 9H)
3	---	---	8.75 (s, 3H)	6.90 (t, J=8.0 Hz, 3H), 7.08 (d, J=7.2 Hz, 3H), 7.26 (s, 3H), 8.73 (s, 3H)	4.3 (br, 3H)	3.19 (s, 9H)	3.62 (s, 9H)
IV	10.95 (br, 3H)	12.92 (s, 3H)	8.70 (s, 3H)	6.73 (t, J=7.8 Hz, 3H), 6.84 (d, J=9.2 Hz, 3H), 7.00 (d, J=9.0 Hz, 3H), 8.65 (s, 3H), 9.27 (s, 3-OH)	---	---	---
4	---	---	8.75 (s, 3H)	6.82 (t, J=7.5 Hz, 3H), 6.91 (d, J=9.0 Hz, 3H), 7.12 (d, J=8.7 Hz, 3H), 8.71 (s, 3H), 9.52 (s, 3-OH)	4.06 (br, 3H)	3.13 (s, 9H)	---
V	11.42 (br, 3H)	12.89 (s, 3H)	8.87 (s, 3H)	7.23 (s, 3H), 7.67 (d, J=2.7 Hz, 3H), 7.43 (dd, J=8.8 Hz, 2.7 Hz 3H), 6.90 (d, J=8.9 Hz, 3H), 8.85 (s, 3H)	---	---	---
5	---	---	9.23 (s, 3H)	7.26 (s, 3H), 7.82 (d, J=2.7 Hz, 3H), 7.57 (dd, J=8.8 Hz, 2.7 Hz 3H), 7.00 (d, J=8.9 Hz, 3H), 9.15 (s, 3H)	4.12 (br, 3H)	3.23 (s, 9H)	---
VI	10.90 (br, 3H)	12.39 (s, 3H)	8.70 (s, 3H)	6.85 (d, J=8.3 Hz, 3H), 7.13 (d, J=9.7 Hz, 3H), 7.42 (s, 3H), 8.68 (s, 3H)	---	---	2.26 (s, 9H)
6	---	---	8.73 (s, 3H)	6.89 (d, J=8.1 Hz, 3H), 7.19 (d, J=8.0 Hz, 3H), 7.43 (s, 3H), 8.71 (s, 3H)	4.08 (br, 3H)	3.19 (s, 9H)	2.21 (s, 9H)
VII	10.27 (br, 3H)	12.44 (s, 3H)	8.39 (s, 3H)	6.34 (d, J=3.5 Hz, 3H), 7.28 (s, 3H), 7.46 (d, J=2.3 Hz, 3H), 8.43 (s, 3H)	---	---	1.12 (s, 18H), 3.36 (s, 12H)
7	---	---	8.73 (s, 3H)	7.31 (s, 3H), 7.48 (d, J=7.2 Hz, 3H), 6.45 (d, J=7.6 Hz, 3H), 8.73 (s, 3H)	4.05 (br, 3H)	3.15 (s, 9H)	1.16 (s, 18H), 3.40 (s, 12H)

Table 5.

Cyclic voltammetric (CV) and differential pulse voltammetric (DPV) results for the ligands and the dioxidomolybdenum(VI) complexes at 298 K.

Compounds ^[a]	<i>E</i> _{pc} [V] ^a	<i>E</i> _{pa} [V] ^a	dpv
I	-1.13, -0.715	0.613	-0.878, 0.486
1	-1.02, -0.732	---	-0.892, -0.112, 0.599
II	-0.841, -0.652	0.360	-0.921, 0.162, 0.773, 1.72
2	-0.932, -0.712	---	-0.855, 0.595, 1.21
III	-1.44, -0.766	1.08	-0.898, 0.260
3	-1.00, -0.744	---	-0.905, 0.409
IV	-0.904, -0.705	1.02	-0.842, 0.938, 1.68
4	-0.930, -0.748	---	-0.874, -0.178
V	-0.752, -0.680	0.829	-0.846, 0.128, 0.738
5	-0.984, -0.748	---	-0.838
VI	-1.07, -0.725	1.00	-0.846, 1.69
6	-1.13, -0.757	---	-0.888, 0.991
VII	-1.34, -0.749	1.21	-0.881, 1.68
7	-1.01, -0.749	---	-0.923, 1.07, 0.477

^a *E*_{pa} and *E*_{pc} are the anodic and cathodic peak potentials vs SCE, respectively.

Table 6.

Conversion of multiple components (0.0050 mol of benzaldehyde, 0.010 mol of ethyl acetoacetate and 0.0050 mol of ammonium acetate) into products (a) and (b) using **1** as a catalyst precursor in 1 h of reaction time under different reaction conditions.

Entry No.	Catalyst [g (mmol)]	Oxidant [g (mmol)]	Temp. [°C]	Solvent (5mL)	Conversion [%]	Selectivity [%] ^a	
						[a]	[b]
1	0.001 (1×10 ⁻³)	0.56 (5)	60	--	65	70	30
2	0.002 (2×10 ⁻³)	0.56 (5)	60	--	70	58	32
3	0.003 (3×10 ⁻³)	0.56 (5)	60	--	72	75	25
4	0.001 (1×10 ⁻³)	1.13 (10)	60	--	82	90	10
5	0.001 (1×10 ⁻³)	1.69 (15)	60	--	84	88	12
6*	0.001 (1×10 ⁻³)	0.56 (5)	30	--	88	100	0
7	0.001 (1×10 ⁻³)	0.56 (5)	40	--	90	98	2
8	0.001 (1×10 ⁻³)	0.56 (5)	50	--	87	96	4
9	0.001 (1×10 ⁻³)	0.56 (5)	30	MeOH	90	65	35
10	0.001 (1×10 ⁻³)	0.56 (5)	40	MeOH	93	62	38
11	0.001 (1×10 ⁻³)	0.56 (5)	30	EtOH	87	70	30
12	0.001 (1×10 ⁻³)	0.56 (5)	30	MeCN	85	62	38
13	0.001 (1×10 ⁻³)	0.56 (5)	30	CH ₂ Cl ₂	82	60	40
14	0.001 (1×10 ⁻³)	0.56 (5)	30	CHCl ₃	78	55	45
15	0.001 (1×10 ⁻³)	0.56 (5)	30	hexane	72	64	36
16	0.001 (1×10 ⁻³)	0.56 (5)	30	DMSO	23	47	53
17	0.001 (1×10 ⁻³)	blank	30	--	46	53	47
19	Blank	blank	30	--	30	20	80
20	Blank	0.56 (5)	30	--	27	38	62
21	Blank		80	--	36	32	68
22	Blank	0.56 (5)	100	--	40	28	72

^a (a) diethyl 2,6-dimethyl-4-phenyl-1,4-dihydropyridine-3,5-dicarboxylate (1,4-DHP) and (b) diethyl 2,6-dimethyl-4-phenylpyridine-3,5-dicarboxylate (Py).

Figures

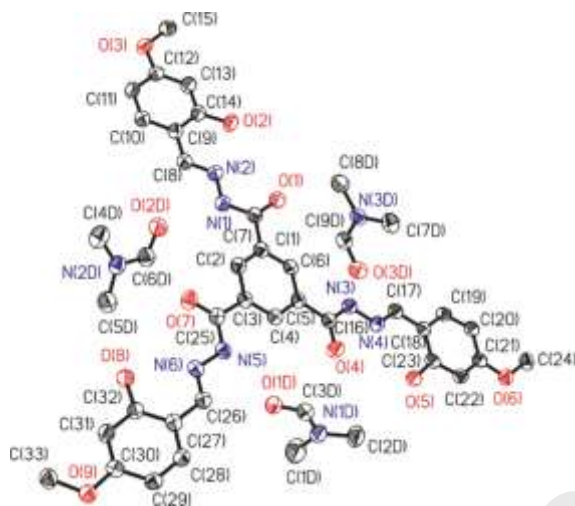


Fig. 1. ORTEP for $H_6L^3 \cdot 3DMF$ (**IIIa**). All the non-hydrogen atoms are presented by their 50% probability ellipsoids. The drawing was done with the SHELXL package [39].

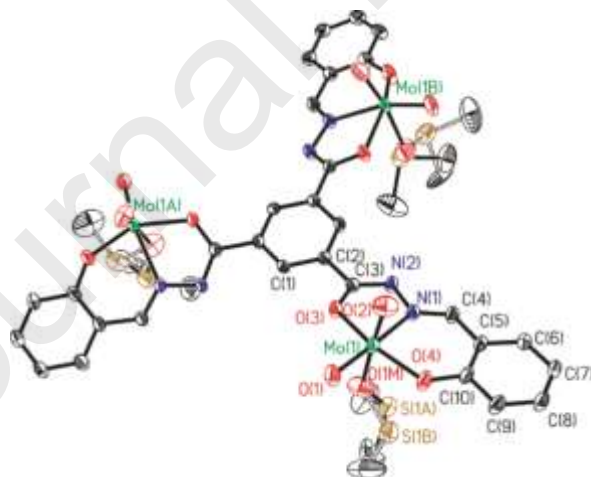


Fig. 2. ORTEP for $[MoO_2(DMSO)_3L]$ (**1a**). All the non-hydrogen atoms are presented by their 50% probability ellipsoids. The drawing was done with the SHELXL package [39].

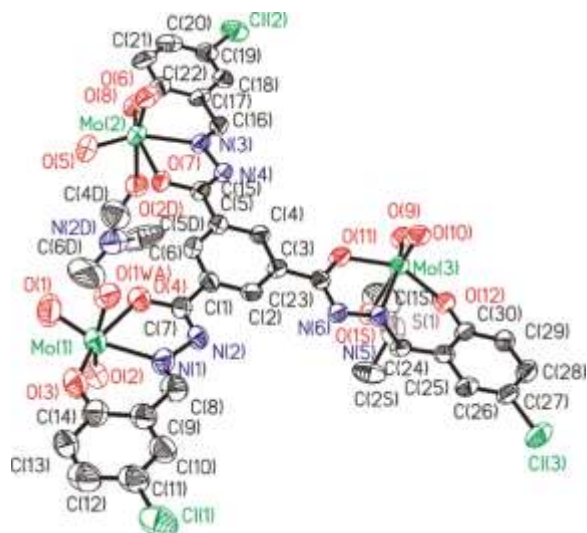


Fig. 3. ORTEP for $[\{\text{MoO}_2(0.5\text{H}_2\text{O}\cdot 0.5\text{MeOH})\}\{\text{MoO}_2(\text{DMF})\}\{\text{MoO}_2(\text{DMSO})\}\text{L}^5]\cdot\text{DMF}\cdot 0.5\text{DMSO}$ (**5a**). All the non-hydrogen atoms are presented by their 50% probability ellipsoids. The drawing was done with the SHELXL package [39].

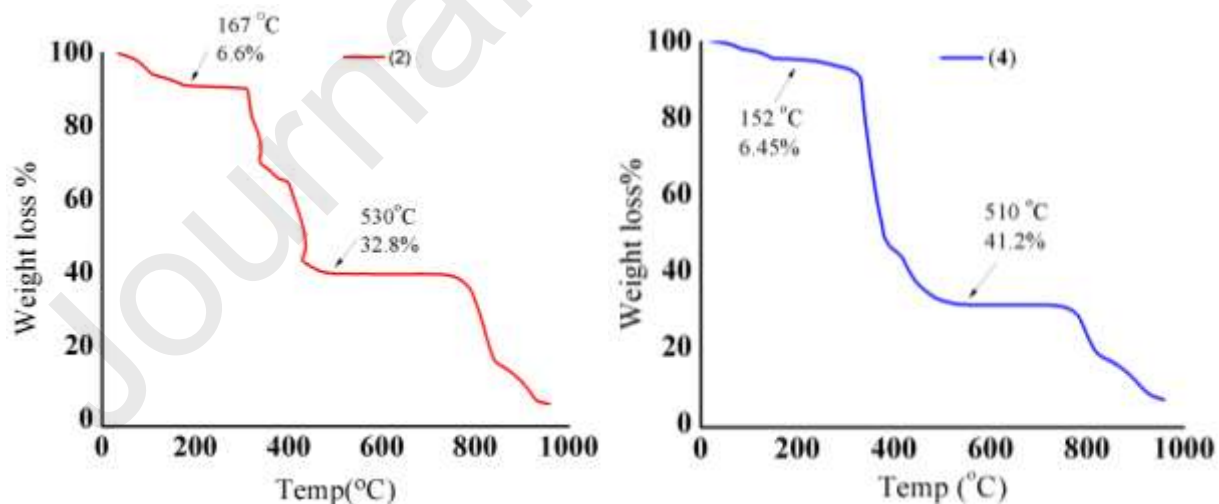


Fig. 4. TGA profiles of complexes **2** and **4**.

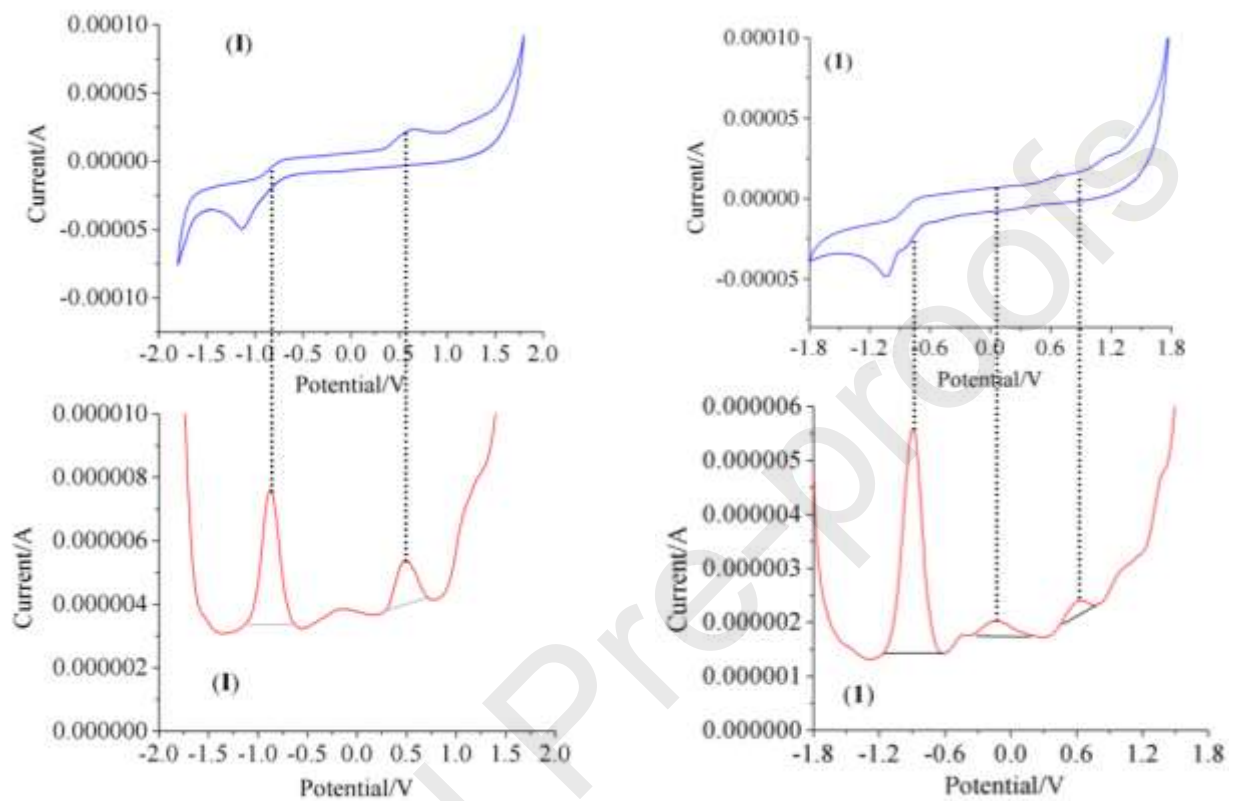


Fig. 5. Comparative study of cyclic voltammetry and differential pulse voltammetry for **I** and **1** (scan rate 100 mV/s) recorded in DMF in the range +2.0 V to -2.0 V vs. Ag/AgCl at room temperature with 0.1 M TBAPF₆ as a supporting electrolyte.

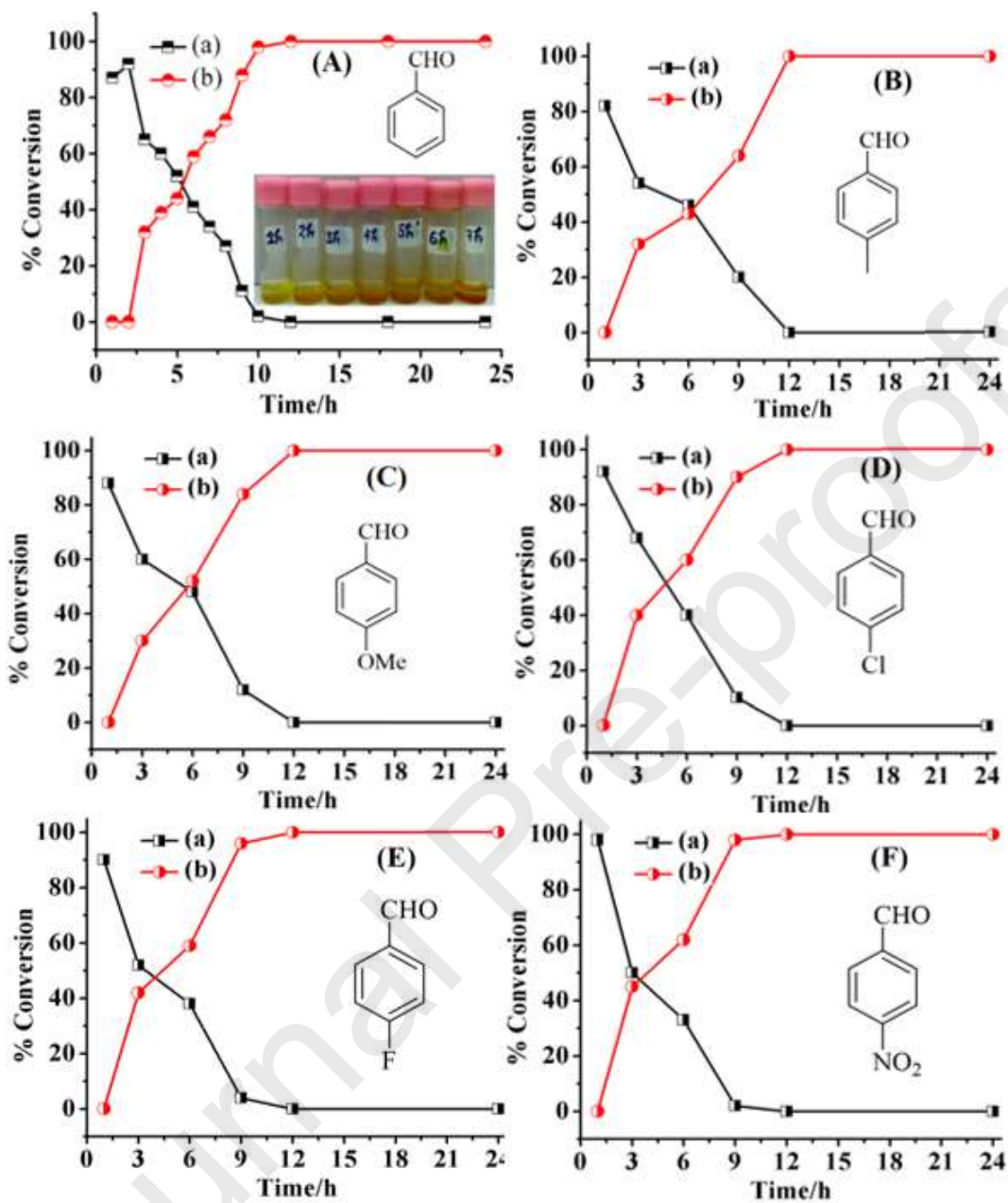


Fig. 6. Reaction profile of the Hantzsch reaction using various aldehydes, ethyl acetoacetate and ammonium acetate under the optimized reaction conditions using **1** as a catalyst.

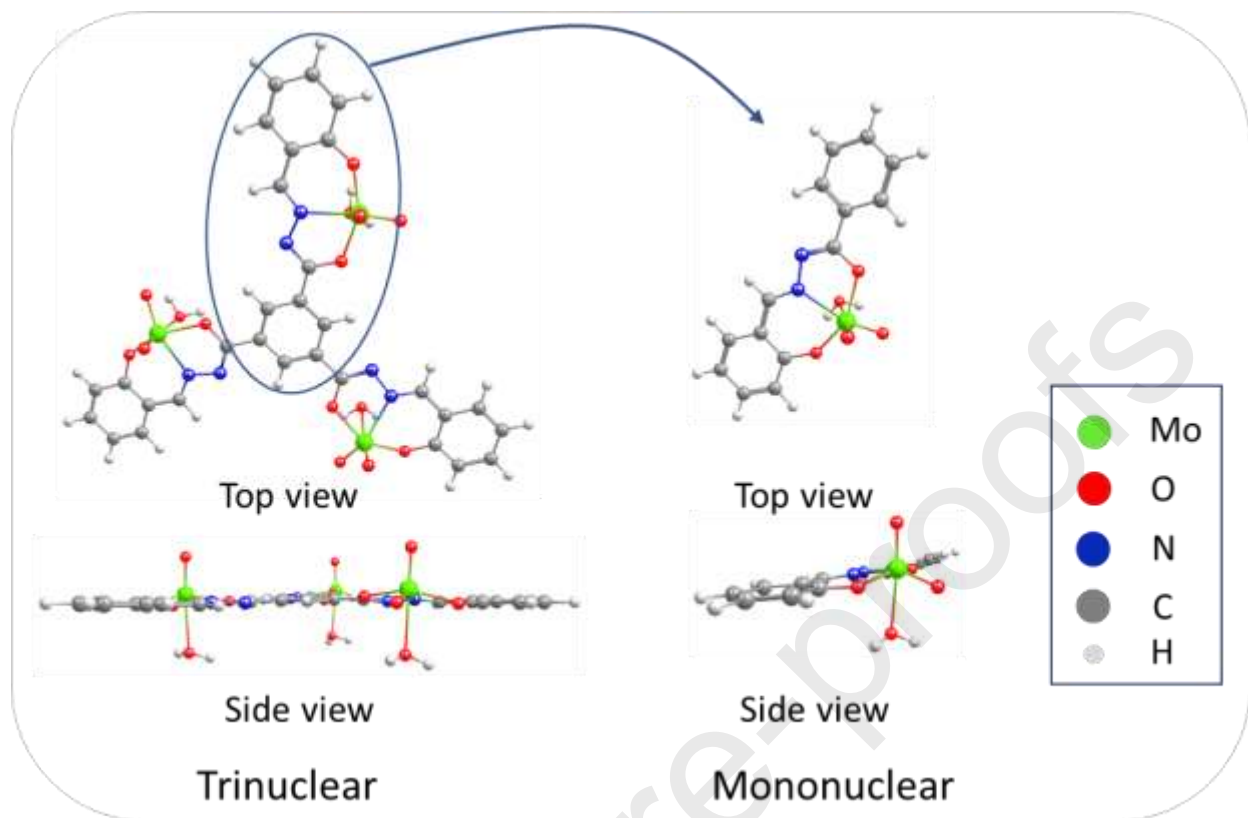


Fig. 7. Geometries of the trinuclear and mononuclear complexes

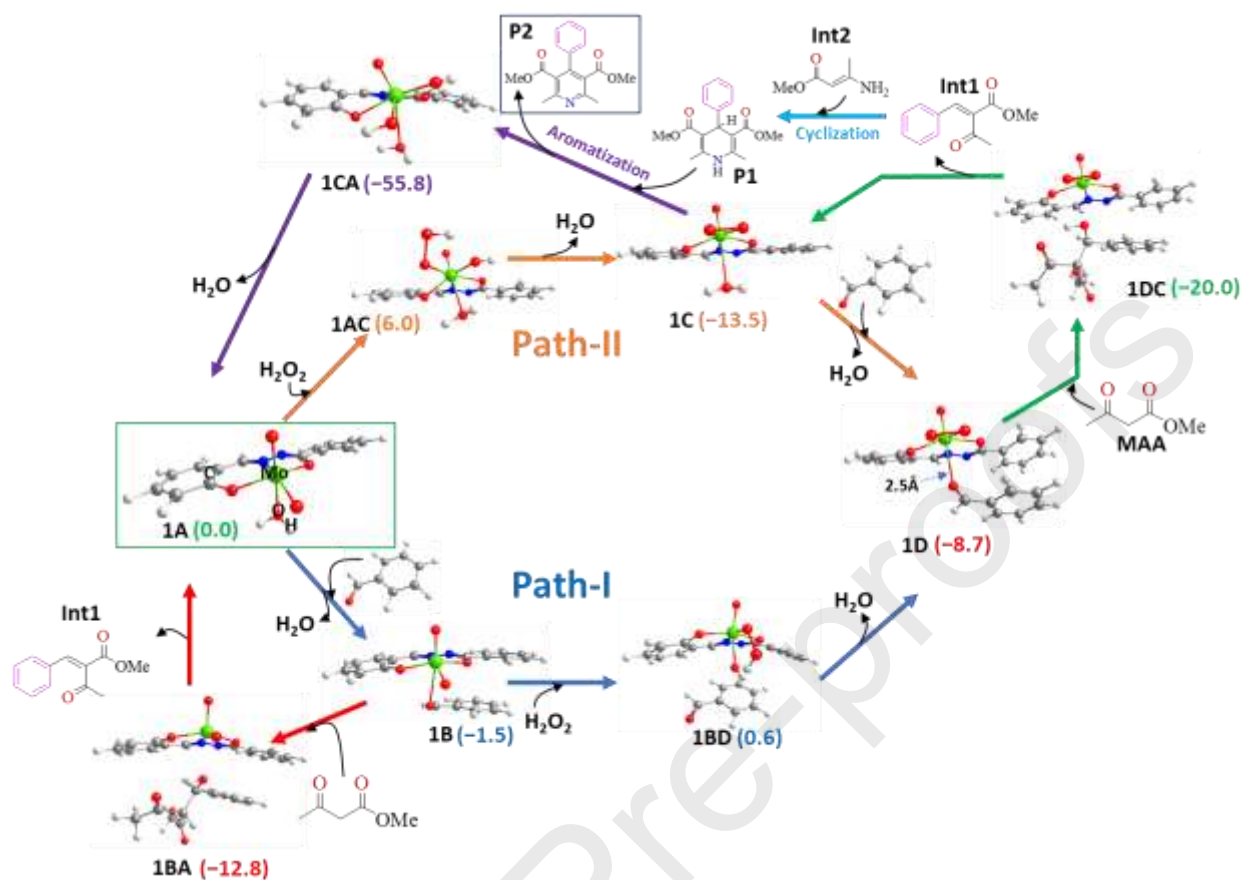
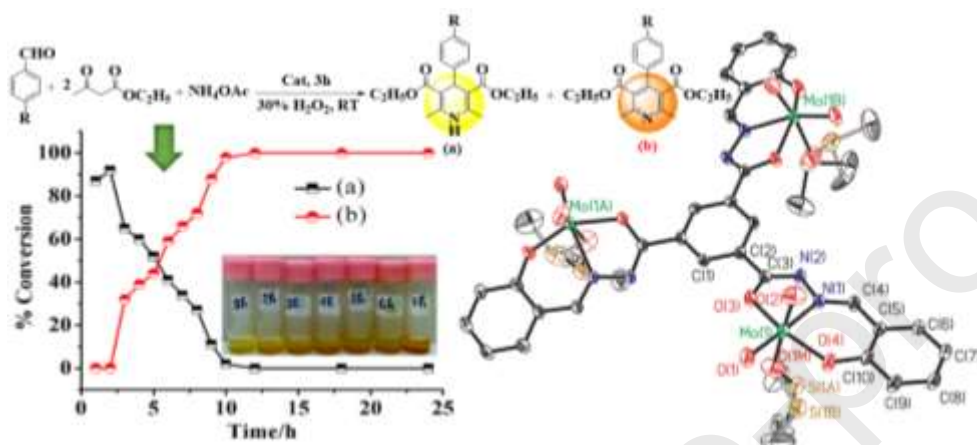


Fig. 8. Pathways **I** and **II** starting from **1(A)** [the dioxidomolybdenum(VI) complex] and leading to the aromatized product (**P2**) via the route of **Int1** and **Int2**. Interactions are studied considering one mononuclear unit of complex **1** as a representative (denoted as **1A**) and substrates, benzaldehyde and methyl acetoacetate. Methyl acetoacetate has been used in place of ethyl acetoacetate to reduce the computational time.

Trinuclear *cis*-dioxidomolybdenum(VI) complexes of compartmental C_3 symmetric ligands: Synthesis, characterization, DFT study and catalytic application for hydroxyridines (Hps) *via* the Hantzsch reaction



Trinuclear *cis*-dioxidomolybdenum(VI) complexes of compartmental C_3 symmetric ligands: Synthesis, characterization, DFT study and catalytic application for hydropyridines (Hps) via the Hantzsch reaction

Mannar R. Maurya, Reshu Tomar, Puneet Gupta, Fernando Avecilla

Trinuclear *cis*-dioxidomolybdenum(VI) complexes of compartmental C_3 symmetric ligands derived from benzene-1,3,5-tricarbohydrazide have been isolated, characterized and tested as catalysts for a one-pot three-components dynamic covalent assembly via the Hantzsch reaction.

There are no conflicts of interest to declare.

Credit Author statement

All authors contribute equally

Journal Pre-proofs